Structural basis for serotonergic regulation of neural circuits in the mouse olfactory bulb

Yoshinori Suzuki[1], Emi Kiyokage[1], Jaerin Sohn[2, 3], Hiroyuki Hioki[2], Kazunori Toida[1, *]

Department of Anatomy, Kawasaki Medical School,
577 Matsushima, Kurashiki, Okayama, 701-0192, Japan[1]

Department of Morphological Brain Science, Graduate School of Medicine, Kyoto University
Yoshidakonoe-cho, Kyoto, 606-8051, Japan[2]

Research Fellow of Japan Society for the Promotion of Science (JSPS),
5-3-1 Koujimachi, Chiyoda-ku, Tokyo, 102-8472, Japan[3]

Abbreviated title: Serotonergic circuits in the olfactory bulb

Associated editor: Prof. Paul E. Sawchenko

Key word: serotonin (5-HT), olfactory bulb, synapse, projection, vesicular glutamate transporter 3

***Corresponding author:** Kazunori Toida, M.D., Ph.D.
Professor and Chairman, Department of Anatomy,
Director, Tissue Biology and Electron Microscopy Research Center, Kawasaki Medical School,
577 Matsushima, Kurashiki, Okayama, 701-0192, Japan
Phone: (+81) 86-462-1111
Fax: (+81) 86-462-1199
E-mail: toida@med.kawasaki-m.ac.jp

Grant support: MEXT/JSPS KAKENHI Grant 24500418; Grant 23500419; Grant 13J01992; Grant 24500408; Grant 25123709. Research Project Grant from Kawasaki Medical School; Grant number: 23E-1; Grant number: 25B-56; Grant number: 25G-5. The Cooperative Study Program of National Institute for Physiological Sciences, Japan for high voltage electron microscopy (H-1250M).

Abbreviation list

3D: three dimensional

5-HT: 5-hydroxytryptamine

-ir: immunoreactive

AAV: adeno-associated virus

ABC: avidin-biotin peroxidase complex

BSA: bovine serum albumin

CB: calbindin

CR: calretinin

DAB: 3,3'-diaminobenzidine tetrahydrochloride

DIO: double inverted open reading frame

DRN: dorsal raphe nucleus

EM: electron microscopy

EPL: external plexiform layer

FLEX: flip-excision

GABA: gamma-aminobutyric acid

GCL: granule cell layer

GFP: green fluorescent protein

GL: glomerular layer

HVEM: high voltage electron microscopy

LD: light:dark

LM: light microscopy

MRN: median raphe nucleus

OB: olfactory bulb

PB: phosphate buffer

PBS: phosphate buffered saline

PCR: polymerase chain reaction

PV: parvalbumin

RT: room temperature

SEM: standard error of the mean

TB: tris buffer

TH: tyrosine hydroxylase

VGAT: vesicular GABA transporter

VGLUT1: vesicular glutamate transporter 1

VGLUT2: vesicular glutamate transporter 2

VGLUT3: vesicular glutamate transporter 3

VIAAT: vesicular inhibitory amino acid transporter

palGFP: palmitoylation site-attached green fluorescent protein

WPRE: woodchuck hepatitis virus posttranscriptional regulatory element

Abstract

Olfactory processing is well known to be regulated by centrifugal afferents from other brain regions, such as noradrenergic, acetylcholinergic, and serotonergic neurons. Serotonergic neurons widely innervate and regulate the functions of various brain regions. In the present study, we focused on serotonergic regulation of the olfactory bulb (OB), one of the most structurally and functionally well-defined brain regions.

Visualization of a single neuron among abundant and dense fibers is essential to characterize and understand neuronal circuits. We accomplished this visualization by successfully labelling and reconstructing serotonin (5-hydroxytryptamine: 5-HT) neurons by infection with sindbis and adeno-associated virus into dorsal raphe nuclei (DRN) of mice. 5-HT synapses were analyzed by correlative confocal laser microscopy and serial-electron microscopy (EM) study. To further characterize 5-HT neuronal and network function, we analyzed whether glutamate was released from 5-HT synaptic terminals using immuno-EM.

Our results are the first visualizations of complete 5-HT neurons and fibers projecting from DRN to the OB with bifurcations. We found that a single 5-HT axon can form synaptic contacts to both type 1 and 2 periglomerular cells within a single glomerulus. Through immunolabeling, we also identified vesicular glutamate transporter 3 in 5-HT neurons terminals, indicating possibly for glutamatergic transmission.

Our present study strongly implicates involvement of brain regions such as the DRN in regulation of the elaborate mechanisms of olfactory processing. We further provide a structure basis of the network for coordinating or linking olfactory encoding with other neural systems, with special attention to serotonergic regulation.

Introduction

The olfactory bulb (OB) is one of the most desirable regions to analyze neuronal organization in the central nervous system due to its simple and distinctly laminar cytoarchitecture, small number of neuron types, and diversity of chemical neuroactive substances. Therefore, the OB is an attractive region to analyze the synaptic organizations of the central nervous system (Halaz and Shepherd, 1983; Shipley and Ennis, 1996; Toida et al., 2008). Neural circuit processing of odor information in the OB is regulated by afferent axons from olfactory receptor neurons. However, there are also other inputs to the OB. Those are centrifugal afferents from other brain regions: noradrenergic neurons from locus coeruleus (Shipley et al., 1985), acetylcholinergic neurons from diagonal band (Zaborszky et al., 1986), and serotonergic neurons from dorsal and median raphe nuclei (DRN and MRN, respectively, McLean and Shipley, 1987).

Serotonergic projections widely innervate the forebrain and are responsible for regulation of various central nervous system functions. Serotonin (5-hydroxytryptamine: 5-HT) is a monoamine neurotransmitter involved in control of behavioral arousal, anxiety, depression, attention, mood, and the autonomic nervous system (Jones and Blackburn, 2002; Hurley et al., 2004; Ptak et al., 2009), and thus attracts variable fields of neurologists and neuroscientists. In spite of such variable neuroactivities, the structural basis, including overall morphology, ultrastructure, and synapses, has not been well established. 5-HT fibers project not only to cortical regions but also to peripheral regions (McLean and Shipley, 1987; Bartolome and Gil-Loyzaga, 2005). The olfactory bulb is one of the most innervated regions by 5-HT fibers from the DRN (McLean et al., 1993; Hardy et al., 2005; Petzold et al., 2009), and therefore, considered a desirable region for analysis of 5-HT neurons. The activity of 5-HT projections from the DRN is the highest before wakefulness and may simultaneously control up-regulation of sensory processing of odors. Depletion of bulbar 5-HT fibers with a specific neurotoxin was followed by the loss of odor discrimination, and the extent of the decrease in the behavioral score of the depleted animals depended on how

the 5-HT fibers disappeared from the OB (Moriizumi et al., 1994), indicating that 5-HT plays a crucial role in olfactory processing.

Two types of transmission determine the effects of 5-HT terminals: synaptic transmission and volume transmission. However, it is still unclear which form of transmission occurs and influences bulbar circuits. Our previous studies showed that presynaptic terminals of unknown origin contained round and dense cored synaptic vesicles and made asymmetrical synapses onto calbindin-immunoreactive (CB-ir, Toida et al., 1998), parvalbumin (PV)-ir (Toida et al., 1994, 1996), and tyrosine hydroxylase (TH)-ir (Toida et al., 2000) neurons with a low rate. These gamma aminobutyric acid (GABA)-immunonegative profiles suggested centrifugal fibers, such as fibers from a 5-HT neuron, that are derived from higher centers (Toida et al., 2008). To understand how 5-HT neurons act on their targets, it is necessary to know formations, regions, and targets of the synapses. Previous studies using electron microscopy (EM) reported that 5-HT neurons made asymmetrical synapses on type 1 and type 2 periglomerular cells in the glomerular layer of the OB. Type 1 periglomerular cells receive synaptic contacts from olfactory receptor neurons and are GABA-immunopositive. Type 2 periglomerular cells do not receive synaptic contacts from olfactory receptor neurons and are GABA-immunonegative (Kosaka and Kosaka, 2005; Gracia-Llanes et al., 2010). Electrophysiological studies showed that 5-HT depolarized a subset of juxtaglomerular cells and projection neurons via 5-HT_{2C} and 5-HT_{2A} receptors, respectively (Hardy et al., 2005; Liu et al., 2012). However, it is unclear whether the origin of those 5-HT fibers is DRN or MRN and how a single 5-HT axon makes synaptic connections with such pleural types of bulbar neurons. Therefore, the aim of the present study was to characterize the steady structural basis for serotonergic regulation in the brain with special focus on the OB neural circuitry by (1) imaging and tracing an entire 5-HT neuron from the origin to the terminal, (2) determining the synaptic contacts 5-HT fibers make throughout all layers, and (3) determining which transmitter is released from 5-HT neurons via synapses.

Materials and Methods

Animals

Thirty four male C57BL/6J mice (8-10 weeks old, weighing 20-25 g), three male Slc6a4-Cre mice (8-10 weeks old, weighing 20-25 g; ET33 and ET127; Gong et al., 2007), and two TH-GFP mice (B6.Cg-Tg(TH-GFP)21-31, Matsushima et al., 2002) were used in this study. C57BL/6J mice were provided by Japan SLC, Inc. The TH-GFP mice were provided by the RIKEN BRC through the National Bio-Resource Project of the MEXT, Japan (RBRC02095). Slc6a4-Cre mice were provided from mutant mouse regional resource center MMRRC supported by NIH (017261-UCD, 017260-UCD). All animals were maintained under 12:12 h light: dark (LD) cycle (lights on 07:00-19:00 h) at ambient temperature (24±1 °C). Food and water were available ad libitum. All animal experiments carried out in this study were approved by the Animal Research Committee of Kawasaki Medical School (approved# 13-034) and by the Committees for Animal Care in Kyoto University (approved# MedKyo 14015) and were conducted according to the "Guide for Care and Use of Laboratory Animals" of Kawasaki Medical School, which is based on the National Institute of Health Guide for the Care and Use of Laboratory Animals (NIH Publications # 80-23) revised 1996. The experiments with sindbis viral vector or adeno-associated viral (AAV) vector and transgenic mice were approved by Recombinant DNA Experiments Safety Committee of Kawasaki Medical School (approved# 12-01) or by the Committees for Recombinant DNA Study in Kyoto University (approved# 120093), respectively.

Production of AAV vector for 5-HT neuron labeling

To achieve cell type-specific expression of a transgene in Cre-expressing 5-HT neurons, we prepared AAV vector with a system of double inverted open reading frame (DIO) or flip-excision (FLEX; Schnütgen et al., 2003) switch. The switch sequence was synthesized *de novo* (GenScript, Piscataway, NJ) and composed of two pairs of loxP and lox2272 sites in opposite orientations. After amplification of palmitoylation site-attached green fluorescent protein (palGFP) by polymerase chain reaction (PCR),

the sequence was introduced between the pairs in the antisense orientation. Then, we inserted the switch sequence containing invertedly orientated palGFP and woodchuck hepatitis virus posttranscriptional regulatory element (WPRE; a gift from Dr. Hope TJ; Zufferey et al., 1999) into pAAV2-MCS (Stratagene, La Jolla, CA), resulting in pAAV2-CMV-DIO-palGFP-WPRE.

Production and purification of the AAV vector were performed according to the previous report (Kataoka et al., 2014) with minor modifications. Briefly, vector and helper plasmids (pXR1, University of North Carolina at Chapel Hill; pHelper, Stratagene) were co-transfected into HEK293T cells (RCB2202, RIKEN BRC, Japan) using polyethylenimine. The medium was replaced 6 h after the transfection with D-MEM (Invitrogen, Eugene, OR) containing 10% fetal bovine serum, 4 mM L-glutamine (Invitrogen), 2 mM GlutaMAX (Invitrogen), 0.1 M Non-Essential Amino acids (Invitrogen), and 1 mM sodium pyruvate (Invitrogen). Sixty hours following medium replacement, cells containing viral particles were collected. The viral particles were purified from a crude lysate of the cells using OptiPrep (Axis-Shield, Oslo, Norway) and then concentrated with Amicon Ultra-15 (NMWL 50K; Millipore, Temecula, CA). Viral titers (transducing units/ml) were adjusted to 1.0×10^{9} TU/ml, and the viral solution was stored in aliquots at –80 ºC until use for delivery to brain tissues.

Selective labeling of 5-HT neuron by viral injection

Twenty four C57BL/6J mice were used for 5-HT labeling with sindbis viral vectors (0.13×10^{10} TU/ml), and three Slc6a4-cre mice were used with AAV vectors. They were anesthetized by intraperitoneal injection of pentobarbital (0.1 ml/100 g body weight). Sindbis viral vectors expressing palGFP in 0.5 μl of phosphate buffered saline (PBS) containing 0.5% bovine serum albumin (BSA) were injected into the DRN (4.1 mm posterior to the bregma, 0.3 mm lateral to the midline, and 2.4 mm deep from the brain surface) of the C57BL/6J mice by pressure through a glass micropipette attached to Picospritzer Ⅲ (General Valve Corporation, East Hanover, NJ). 0.5 μl of the viral vectors AAV2/1 CMV-DIO-palGFP-WPRE were injected into the DRN (4.0 mm

posterior, 0.0 mm lateral, and 2.9 mm deep) of Slc6a4-Cre mice. These transgenic mice express Cre recombinase specifically in 5-HT neurons, thus only 5-HT neurons were labeled with palGFP by viral injection/infection. The sindbis virus-injected mice were perfused 96 h after the injection, and the AAV-injected mice were perfused 7 days after injection. They were anesthetized by intraperitoneal injection of sodium pentobarbital (0.1 ml/100 g body weight) and perfused transcardially with a fixative containing 4% paraformaldehyde and 0.05% glutaraldehyde in 0.1 M phosphate buffer, pH 7.4 (PB). Brains were dissected out after perfusion and postfixed with the same fixative. The brains were then cut serially in 50-μm thick parasagittal sections on a microtome (VT 1200S, Leica, Germany) and collected serially in PBS.

Characterization and visualization of palGFP-expressing DRN neurons

Sindbis viral vectors can infect every neuron and glia. Therefore, we examined whether infected cells were 5-HT immunoreactive. The sections were observed under a fluorescence microscope (BX61, Olympus, Japan) to find successfully infected DRN neurons. Sections containing palGFP-positive neurons were selected and incubated in blocking solution containing 1% BSA, 0.3% Triton X-100, and 0.5% sodium azide in PBS for 1 h at 20 °C. Then, they were incubated in rabbit anti-5-HT IgG (ImmunoStar, Inc. Cat# 20080 RRID:AB_572263) diluted 1:50,000 and chicken anti-GFP IgY (Life Technologies Cat# A10262 RRID:AB_11180610) diluted 1:10,000 in BSA for 5 days at 20 °C. The sections were incubated in biotinylated donkey anti-chicken IgY (Jackson Immunoresearch Cat# 703-065-155 RRID:AB_2313596) diluted 1:200 in BSA containing 0.3% Triton X-100 for 2 h at 20 °C. They were then incubated in Alexa 568-conjugated streptavidin (Invitrogen Cat# S11226 RRID:AB_2315774) diluted 1:200 and Dylight 649-conjugated donkey anti-rabbit IgG (Jackson Cat# 711-495-152 RRID:AB_2315775) diluted 1:200 in BSA containing 0.3% Triton X-100 for 2 h at 20 °C. Sections were carefully rinsed in PBS (3×10 min) after each step. Finally, sections were mounted on glass slides and cover slips with VECTASHIELD (Vector Laboratories, Burlingame, CA). Sections were analyzed under two-photon

laser microscopy (Leica SP2, Germany).

The brain sections of sindbis virus-injected mice containing fibers immunopositive for both GFP and 5-HT, and those of AAV-injected mice containing fibers fluoropositive for GFP were visualized by the avidin-biotin peroxidase complex (ABC). All serial sections were incubated in blocking solution for 1 h at 20 °C and in chicken anti-GFP diluted 1:10,000 in blocking solution overnight at 20 °C. They were incubated in biotinylated donkey anti-chicken IgY diluted 1:200 in BSA containing 0.3% Triton X-100 for 2 h at 20 °C and then in ABC (elite variety, Vector) diluted 1:200 in PBS for 2 h at 20 °C. The peroxidase reaction was visualized using 0.05% 3,3'-diaminobenzidine tetrahydrochloride (DAB) (Dojindo, Kumamoto, Japan) and 0.01% H_2O_2 in Tris buffer (TB, pH 7.6) for 3 min at room temperature (RT). After a PB rinse, they were treated with 0.05% osmium tetroxide in 0.1 M PB for 30 min at 4 °C and then washed in H_2O. The sections were then dehydrated through graded ethanol series, infiltrated in propylene oxide, and flat-embedded in Epon-Araldite (TAAB, UK).

Immunohistochemistry

Five C57BL/6J mice were used for light microscopy (LM), and seven mice (five C57BL/6J and two TH-GFP mice) were used for correlative confocal laser microscopy (CLSM) and serial-EM. They were anesthetized by intraperitoneal injection of pentobarbital (0.1ml/100 g body weight) and perfused transcardially with a fixative containing 4% paraformaldehyde and 0.1 M phosphate buffer, pH 7.4 (PB). The brains of the animals were dissected out after perfusion and postfixed with the same fixative. The brains were cut serially in 50-μm thick parasagittal sections on a microtome (VT 1200S, Leica, Germany) and corrected serially in PBS.

In this study, we used blocking solution containing 1% BSA, 0.3% Triton X-100, and 0.5% sodium azide in PBS for LM and high voltage electron microscopy (HVEM), and containing 1% BSA and 0.5% sodium azide in PBS for EM. Sections for LM were incubated in blocking solution for 1 h at 20 °C and in rabbit anti-5-HT IgG

diluted 1:50,000 in 1% BSA for 5 days at 20 °C. After rinse in PBS, they were incubated in biotinylated horse anti-rabbit IgG diluted 1:200 in blocking solution for 2 h at 20 °C and ABC (standard variety) diluted 1:200 in PBS for 2 h at 20 °C. The peroxidase reaction was visualized using DAB and 0.01% H_2O_2 in TB for 3 min at RT. After rinse in PB, they were treated with 0.1% osmium tetroxide in 0.1 M PB for 1 h at 4 °C and washed in H_2O. The slides were dehydrated through graded ethanol series, infiltrated in propylene oxide, and flat-embedded in Epon-Araldite.

For detecting contact with other specific neurons or co-expression of other neuroactive substances, sections were incubated in blocking solution in PBS for 1 h at 20 °C. Primary antibodies used in the present study were as follows: (1) rabbit anti-5-HT IgG (diluted 1:50,000); (2) mouse anti-CB IgG (diluted 1:5,000, Swant Cat# 300 RRID:AB_10000347); (3) guinea pig anti-vesicular glutamate transporter 3 (VGLUT3) IgG (diluted 1:200, Hioki et al., 2004 Cat# VGLUT3 RRID:AB_2315581); (4) mouse anti-tyrosine hydroxylase (TH) IgG (diluted 1:5,000, Chemicon Cat# MAB318 RRID:AB_2315522); (5) goat anti-calretinin (CR) IgG (diluted 1:5,000, Millipore Cat# AB1550 RRID:AB_90764); (6) guinea pig anti-vesicular glutamate transporter 1 (VGLUT1) (Kyoto University (Fujiyama et al., 2001; Hioki et al., 2003) Cat# VGLUT1 (vesicular glutamate transporter 1) RRID:AB_2315554); (7) guinea pig anti-vesicular glutamate transporter 2 (VGLUT2) (Kyoto University (Fujiyama et al., 2001; Hioki et al., 2003) Cat# VGLUT2 (vesicular glutamate transporter 2) RRID:AB_2315571) in blocking solution for 5 days at 20 °C. Combinations of two or three different antibodies selected from rabbit, goat, mouse, and guinea pig were used for multiple immunolabeling. After incubation in mixtures of the primary antibodies, the sections were then incubated in mixtures of the following secondary antibodies for 2 h at 20 °C: (1) FITC-conjugated donkey anti-rabbit IgG (diluted 1:200, Jackson Cat# 711-095-152 RRID:AB_2315776); (2) Cy3-conjugated horse anti-mouse IgG (diluted 1:200, Jackson Cat# 715-165-151 RRID:AB_2315777); (3) Cy3-conjugated donkey anti-guinea pig IgG (diluted 1:200, Jackson Cat# 706-165-148); (4) Cy3-conjugated donkey anti-sheep IgG (diluted 1:200, Jackson Cat# 713-165-147 RRID:AB_2315778)

in blocking solution. After rinse in PBS, they were mounted on slides and cover slips with VECTASHIELD Mounting Medium (Vector Laboratories, Burlingame, CA). The slides were analyzed under two photon laser microscopy (SP2; x63/NA 1.4 plan-apochromat objective lens) or confocal laser microscopy (CLSM, zeiss LSM700; x63/NA 1.4 plan-apochromat objective lens, or Nikon A1R-MP, x25/NA 1.1 apochromat objective lens) with digital zoom mode.

High-voltage electron microscopy

After blocking, sections were incubated in rabbit anti-5-HT IgG diluted 1:50,000 in 1% BSA for 5 days at 20 °C. After rinse in PBS, they were incubated in biotinylated horse anti-rabbit IgG diluted 1:200 in 1% BSA containing 0.3% Triton X-100 and 0.5% sodium azide for 2 h at 20 °C and ABC (elite variety) diluted 1:200 in PBS for 2 h at 20 °C. After rinse in TB, the peroxidase reaction was visualized using Metal Enhanced DAB Substrate Kit (cat# 34065, Thermo scientific, Japan) for 5 min at RT. Some samples exhibiting complexity of arborization by 5-HT immunostained axons were selected for HVEM with its high power resolution. They were rinsed in PB and post-fixed with 3% glutaraldehyde in 0.1 M PB for 30 min and 1% osmium tetroxide for 1 h at 4 °C. The slides were dehydrated through graded ethanol series, infiltrated in propylene oxide, and flat-embedded in Epon-Araldite. From these sections, 3-μm-thick sections were cut with an ultramicrotome, mounted on mesh grids (D-75, VECO Holland), and examined with an HVEM (Hitachi H-1250M in National Institute for Physiological Science, Okazaki, Japan) at an accelerating voltage of 1,000 kV. Stereo-paired images were prepared by tilting the specimen stages ± 8 degrees compared to the prerecorded LM images. The HVEM method in detail has been described in our previous study (Toida et al., 1998).

Three-dimensional reconstruction of single 5-HT neurons

DAB-visualized 5-HT neurons were digitally traced and reconstructed with Neurolucida 11.0 software (Micro Bright Field, RRID:nif-0000-10294) and a

microscope (BX61, Olympus, Japan) equipped with a CCD camera (Retiga 2000R, QImaging, CA). Some samples were also analyzed with Lucivid-006 (Micro Bright Field) using a microscope (BX50, Olympus, x100/NA1.4oil plan-apochromat objective lens) and Neurolucida 11.0 software.

Electron microscopy and electron tomography

After immunostaining sections with rabbit anti-5-HT antibody as described above, the sections were treated with 1% osmium tetroxide in 0.1 M PB for 1 h at 4 °C and then washed with dH_2O. They were then treated with 2% aqueous uranyl acetate for 30 min at 4 °C and washed with dH_2O. The sections were dehydrated through graded ethanol series, infiltrated in propylene oxide, and flat-embedded in Epon-Araldite. From these samples, thin sections 75 nm in thickness were cut with an ultramicrotome (Reichert-Nissei Ultra-Cuts, Leica, Germany) and examined with a digital transmission EM (JEM-1400, JEOL, Japan).

To detect by EM the target of the 5-HT synapse and the neurotransmitter(s) contained in the synaptic vesicles, sections were incubated in 1% BSA for 1 h at 20 °C and in rabbit anti-5-HT IgG diluted 1:50,000 and mouse anti-CB IgG diluted 1:5,000, mouse anti-TH IgG diluted 1:5,000, goat anti-CR IgG diluted 1:5,000, or guinea pig anti-VGLUT3 IgG diluted 1:200 in 1% BSA for 5 days at 20 °C. After rinse in PBS, they were incubated in biotinylated horse anti-mouse IgG (diluted 1:200, Vector Laboratories Cat# BA2000 RRID:AB_2313581), biotinylated horse anti-goat IgG (diluted 1:200, Vector Laboratories Cat# BA9500 RRID:AB_2313580), or biotinylated donkey anti-guinea pig IgG (diluted 1:200, Jackson Cat# 712-065-153 RRID:AB_2315779) in BSA for 2 h at 20 °C. After PBS rinse, the sections were incubated in Alexa Fluor-594 FluoroNanogold-conjugated streptavidin (diluted 1:200, Nanoprobes Cat#7316 RRID:AB_2315780) and FITC-conjugated horse anti-rabbit (diluted 1:200,Jackson Cat# 711-095-152 RRID:AB_2315776) in BSA for 2 h at 20 °C. After rinse in PBS, they were incubated rabbit Peroxidase-anti-peroxidase complex (diluted 1:200, Jackson Cat# 323-005-024 RRID:AB_231578) overnight at 20 °C. The

peroxidase reaction was visualized using DAB and 0.01 % H_2O_2 in TB for 20 min at RT. The gold immunoparticle staining was improved using a silver enhancement kit (HQ silver, Nanoprobes) for 4 min at RT in the dark. After treatment with 1% osmium and 2% aqueous uranyl acetate, the slides were dehydrated through graded ethanol series, infiltrated in propylene oxide, and flat-embedded in Epon-Araldite. From these samples, thin sections 75 nm in thickness were cut serially with an ultramicrotome and examined by EM. Immuno-EM methods have been described in our previous studies (Toida et al., 1996, 1998, 2000). 5-HT synapses were analyzed with electron tomography to examine fine synaptic structures in more detail. Tilt series were recorded with the TEM recorder (Ver. 2.32, JEOL, Japan) from +65° to -35° with 1° steps and reconstructed by tomography (TEMography software (Ver. 2.7, System In Frontier INC., Japan)). Composer software (Ver. 3.0, System In Frontier INC.) and Visualizer-kai software (ver. 1.5, System In Frontier INC.) were also used to display reconstruction data. Thus, 360° rotation by 1° step and 0.5 nm step reslice images could be obtained from three dimensional (3D) voxel data.

Correlative CLSM and serial sectioning EM for 3D reconstruction of 5-HT axons

We reconstructed 5-HT axons from serial EM sections combined with CLSM images to examine whether a single 5-HT axon targets multiple types of interneurons. Sections of TH-GFP mouse were incubated in blocking solution for 1 h at 20 °C and in rabbit anti-5-HT IgG diluted 1:50,000, mouse anti-TH IgG diluted 1:5,000, and goat anti-CB (Santa Cruz Biotechnology Cat# sc-7691 RRID:AB_634520) IgG diluted 1:5,000 in 1% BSA for 5 days at 20 °C. They were incubated in biotinylated goat anti-rabbit IgG diluted 1:200 in BSA for 2 h at 20 °C. They were incubated in FITC-conjugated donkey anti-mouse IgG (Jackson Cat# 715-095-151 RRID:AB_2335588) diluted 1:200, Dylight 649-conjugated donkey anti-sheep IgG (Jackson Cat# 713-495-147 RRID:AB_2335589) diluted 1:200, and Alexa 568-conjugated streptavidin diluted 1:200 in blocking solution for 2 h at 20 °C. After each step, the sections were rinsed in PBS. They were mounted on slides and cover slips with VECTASHIELD Mounting

Medium, and analyzed by LSM700 (x63/NA 1.4 plan-apochromat objective lens). After serial confocal images were stacked and recorded, immunostained sections for the CLSM were rinsed in PBS. Subsequently, the sections were used for EM samples as described above. A series of 100 serial ultra-thin sections, each 75 nm in thickness, were cut and examined with a digital EM (JEM-1400). A large montage that was made of 225 images (15 × 15 images) covered an observation area using CLSM. Each image was taken photo at magnification 6,000× which could recognize synaptic vesicles and clefts (4.2 nm/pixel, 1,024 pixels × 1,024 pixels of each image). DAB-labeled 5-HT axons in a series of montages were reconstructed with Neurolucida 11.0 software. These serial-sectioning and 3D-reconstruction EM studies generally followed our previous studies (Toida et al., 1998, 2000).

Image analysis

5-HT-ir axons were reconstructed with Neurolucida 11.0 software (Micro Bright Field) and a microscope (BX61) equipped with a CCD camera (Retiga 2000R). Serotonergic fiber density in each layer was measured using Photoshop software (version 9.0, Adobe Systems INC., San Jose, CA), as previously described (Gomez et al., 2012). Briefly, digital images were taken from 5 randomly selected areas. The images were treated to balance the signal-to-noise ratio in such a way that the positive elements were clearly distinguishable from the background. That is, the images were manually transformed into binary images in which only immunostained elements appeared as white pixels. After this, fiber density was calculated as the white/black pixel ratio.

The length and number of bifurcations and varicosities from digital reconstruction data for LM were measured with Neurolucida Explorer 11.0 software (Micro Bright Field). Thickness of postsynaptic densities of 5-HT neurons and olfactory receptor neurons were measured with the scale bar of the EM images. The diameters of varicosities and non-varicosity portions were measured on HVEM images.

Statistical analysis

Density differences of 5-HT neurons among the layers, the number of varicosities per 50 μm length on 3D-traced fiber among the layers, and the number of bifurcations among the layers were assessed using student's t test. Differences in thickness of postsynaptic density of 5-HT neurons and olfactory receptor neurons were assessed using Levene tests and Welch tests. Differences were considered statistically significant at $p < 0.05$. Statistical analysis was performed using JMP software (ver. 9, SAS Institute Inc., North Carolina, USA.). Mean ± standard error of the mean (SEM) were used throughout the text as central tendency and dispersion measure, respectively.

Antibody characterization

Table 1 lists all primary antibodies used in this study. All antibodies have been previously characterized and performed well in previous studies.

The 5-HT antibody recognized serotonin coupled to bovine serum albumin (BSA) with paraformaldehyde (manufacturer's product information sheet). The pattern of distribution was consistent with the thorough description of the 5-HT immunoreactivity in a previous study (Bregman, 1987a).

The GFP antibody was raised against GFP isolated directly from Aequorea victoria, and the IgY fraction is purified by affinity purification. The chicken IgY lacks a classic "Fc" domain and does not bind to mammalian IgG Fc receptors, resulting in lower backgrounds during immunostaining protocols (manufacturer's product information sheet). The immunostaining pattern was consistent with the previous studies (Takashima et al., 2007).

The VGLUT1 antibody recognized a single band of 58 kDa by western blot and stained neuropil in layers Ⅰ, Ⅳ, and Ⅵ of the rat neocortex. When the primary antibodies were absorbed with an excess amount of their antigen peptides, no immunoreactivity was found in any the cortical regions (Fujiyama et al., 2001).

The VGLUT2 antibody recognized a single band of 62 kDa by western blot and stained neuropil in layers Ⅰ, Ⅱ, Ⅲ, and Ⅴ intensely and layer Ⅳ moderately of

the rat neocortex. When the primary antibodies were absorbed with an excess amount of their antigen peptides, no immunoreactivity was found in any the cortical regions (Fujiyama et al., 2001).

The VGLUT3 antibody recognized a single band that was in register with molecular weight of VGLUT3. The peptide corresponding to the C-terminal 25 amino acids of rat VGLUT3 was synthesized with addition of N-terminal cysteine for coupling of the peptide with a carrier protein. The antisera were then affinity purified by column chromatography with an antigen-conjugated column. When the primary antibody was preincubated with an excess amount of the antigen peptide, no immunoreactivity was observed on the rat tissue sections (Hioki et al., 2004).

The TH antibody was produced against TH purified from PC12 cells and recognized an epitope on the outside of the regulatory N-terminus and a protein of approximately 59-61 kDa by Western blot. It did not react with dopamine-beta-hydroxylase, phenylalanine hydroxylase, tryptophan hydroxylase, dehydropteridine reductase, sepiapterin reductase, or phenethanoalamine-N-methyl transferase on western blots, and the staining pattern was consistent with previous reports (manufacturer's product information sheet; Collier et al., 1999; Lazarenko et al., 2009).

The CR antibody recognized approximately 30 kDa by Western blots of rat brain extracts. This antibody stains subtypes of amacrine cells, including cholinergic amacrine cells in mouse and rat retina (Puthussery et al., 2010).

The CB monoclonal antibody is a mouse IgG1 produced by hybridization of mouse myeloma cells with spleen cells from mice immunized with calbindin D-28k purified from chicken gut (Celio et al., 1990). It recognized a single band of 28 kDa by western blot. This antibody stains the ^{45}Ca-binding spot of calbindin D-28k (MW 28,000, IEP 4.8) in a two-dimensional gel (manufacturer's product information sheet).

The CB polyclonal antibody was raised against a peptide mapping at the C-terminus of Calbindin D28K of human origin. It recognized a band of approximately 29 kDa on western blot (manufacturer’s product information sheet). The staining

pattern was consistent with the previous report (Nakamura et al., 2004).

Results

Variable distribution of 5-HT neurons throughout OB layers

5-HT immunoreactivity was intense throughout the OB. The most remarkable immunoreactivity for 5-HT was observed in the glomerular layer (GL), moderate immunoreactivity was observed in the granule cell layer (GCL), and the lowest immunoreactivity was observed in the external plexiform layer (EPL, Fig. 1A). These results correlate well with previous data in rats (Takeuchi et al., 1982; Mclean and Shipley, 1987; Gomez et al., 2005; Gracia-Llanes et al., 2010).

In the GL, 5-HT fibers were distributed both in periglomerular regions and in the glomerulus with frequent varicosities and bifurcations at various intervals (Fig. 1B). Many fibers were tortuous and intermingled, so each fiber could not be distinguished. In the EPL, there were few bifurcations, and fibers ran vertically from the GCL to the GL (Fig. 1C). In the GCL, fibers traveled in parallel and vertical to the layer with bifurcations to the GL (Fig. 1D). Generally, thickness of the fibers was similar throughout layers. There were statistical differences in the densities of 5-HT fibers (pixel ratio) among the layers (3.4 ± 0.41 in the GL, 0.33 ± 0.29 in the EPL, 0.69 ± 0.028 in the GCL: GL vs EPL; $p < 0.05$, EPL vs GCL; $p = 0.55$, GL vs GCL; $p < 0.05$, Fig. 2). The distribution of 5-HT axons with bifurcations and varicosities within the glomerulus or at periglomerular region was confirmed by HVEM observation (Fig. 1E and 1F). In addition, HVEM clearly revealed accurate diameters of varicosities and non-varicosity portions of 5-HT fibers (0.86 ± 0.032 μm and 0.27 ± 0.019 μm, n=10, respectively).

5-HT axons in the olfactory bulb were further characterized by morphological analyses of varicosity and branch number through the OB layers (Fig. 3, 4). Fibers branched in each layer with the majority in the GL and the least in the EPL. Branches distributed among several glomeruli. Morphometry of these neuronal fibers is summarized in Table 2. There were no statistical differences between the layers regarding the number of varicosities per 50 μm of axon (3.64 ± 0.16 in the GL, 4.18 ± 0.60 in the EPL, and 2.96 ± 0.45 in the GCL: GL vs. EPL; $p = 0.42$, EPL vs. GCL; p

= 0.08, GL vs. GCL; p = 0.31) (Fig. 4C). However, there were statistical differences between the layers regarding the number of the bifurcations (9.5 ± 1.04 in the GL, 1.25 ± 0.48 in the EPL, and 3.75 ± 1.03 in the GCL: GL vs. EPL; $p < 0.05$, EPL vs. GCL; p = 0.078, GL vs. GCL; $p < 0.05$, Fig. 4D).

Single 5-HT neuron tracing from DRN to the OB

Neuron labeling methods with viral vectors are useful for single neuron tracing studies (Kuramoto et al., 2009; Ohno et al., 2012). To clarify projection pathways of a single 5-HT neuron, the DRN neurons were visualized by stereotaxic injection of viral vectors of sindbis virus or of AAV. In the wild type mouse infected with sindbis virus, we selected neurons that were GFP-ir and 5-HT-ir in the DRN (Fig. 5A and B), traced entire axons to the olfactory bulb, and three-dimensionally reconstructed the fibers. We traced nine 5-HT fibers and showed representative data in Fig. 5C, D, and E. Reconstruction of projections revealed that axon projecting patterns started from DRN, went through the red nucleus in the medial ventral direction, entered the medial hypothalamic nucleus, turned within the anterior hypothalamic nucleus in the lateral direction avoiding the medial preoptic nucleus, entered the accumbens nucleus, reaching anterior olfactory cortex, and finally neared the entrance of the OB. There were no axons found through any of the layers of OB in this case. Some of the axons bifurcating at the red nucleus and medial hypothalamic nucleus projected back toward the DRN. Total length of the representative axon was 23,320 μm, and the single axon fiber bifurcated 14 times. In the Slc6a4-Cre transgenic mouse infected by AAV, we confirmed that all infected neurons in the DRN were 5-HT-ir (Fig. 5J). The axonal projection pattern was similar as sindbis virus-infected axons. Bifurcations were found at the anterior olfactory cortex and accumbens nucleus. The branches terminated at the lateral septal nucleus, infralimbic nucleus, and anterior olfactory nucleus with varicosities (Fig. 5G, H, I and supplementary data 1). Total length of the representative axon was 25,900 μm, and the axon bifurcated 15 times. The varicosities were seen only in the terminals. In the OB, the axon branched two times in the GCL, passed through

the EPL without bifurcations, and reached the GL distributing in two glomeruli (Fig. 5F). The branches in the GCL did not reach the GL. 5-HT fibers analyzed in the present study were categorized as thin fibers. Thus, for the first time, a single tracing analysis revealed the complete projection pattern of a single 5-HT neuron.

Variable synapses formed by 5-HT neurons in the OB

To reveal 5-HT neuronal circuitry in the OB, we used EM analysis to examine synaptic formations by 5-HT-ir axons in each OB layer.

In the olfactory nerve layer, there were few 5-HT-ir axons and no synapses between 5-HT-ir axons and olfactory nerves. In the GL, 5-HT-ir axons made synapses onto the dendrites of interneurons (Fig. 6A). All synapses in the GL were classified as asymmetrical synapses having a clear active zone and heterogeneous sized vesicles at the presynaptic site. A vast majority of the vesicles were round in shape, with some flattened vesicles. A small number of dense cored vesicles were also found. Postsynaptic densities exhibited various features. In the EPL, the mitral cell layer, and the internal plexiform layer, we have not yet observed synapses by 5-HT-ir axons onto dendrites or cell bodies of projection neurons or interneurons. In the GCL, 5-HT-ir axons again made synapses onto the dendrites of interneurons (Fig. 6B). Synapses in the GCL were similar to those in the GL. All synapses existed at varicosities on the fibers, whereas 28% of varicosities reconstructed had synaptic contacts (10 synapses / 35 varicosities).

To further clarify synaptic formations, the synapses of 5-HT neurons were analyzed by electron tomography. The stereo pair at +10° and +26° revealed that there was a clear synaptic cleft (Fig. 6D and 6E). A 0.5 nm-step image obtained by electron tomography showed that the synaptic cleft was well differentiated to be identified as an asymmetrical synapse (Fig. 6F and supplementary data 2). 5-HT postsynaptic densities exhibit morphological differences compared to olfactory receptor neurons (Fig. 6C).

To demonstrate distinctive features of 5-HT synapses and olfactory receptor neuron synapses, we compared their postsynaptic densities by electron tomography.

The thickness of postsynaptic densities of 5-HT neurons and olfactory receptor neurons were 32 ± 2.4 nm and 37 ± 1.1 nm, respectively, showing a statistical difference about the variance, correlative to standard error of the mean, of the postsynaptic densities; thickness of 5-HT PSDs distributed in wider range than olfactory receptor neurons ($F = 8.4$, $p = 0.006$, Levene test). Moreover, there was a statistical difference between mean of the thickness of the postsynaptic density; 5-HT synapses had thinner PSDs than olfactory receptor neurons ($p=0.04$, Welch test, Fig. 7).

Heterogeneous targets of synapses from 5-HT neurons in the OB

To identify the target neurons of 5-HT axons in the OB, we immunostained for 5-HT and markers of bulbar interneurons. Results showed that 5-HT-ir axons contacted dendrites and somata of interneuron subpopulations: CB-ir neurons (Fig. 8A), TH-ir neurons (Fig. 8B), and CR-ir neurons (Fig. 8C), all in the GL, and CR-ir neurons (Fig. 8D) in the GCL. We further analyzed, by correlative CLSM and serial-EM, whether contacts between 5-HT neurons and interneurons form synapses. 5-HT-ir axons made asymmetrical synapses onto the dendrites of CB-ir neurons (Fig. 8A1), TH-ir neurons (Fig. 8B1), and CR-ir neurons (Fig. 8C1) in the GL, and made asymmetrical synapses to CR-ir neurons (Fig. 8D1) in the GCL. At the LM level, 5-HT neurons contact soma of interneurons, but we have not yet observed synaptic connections.

In the present tracing study, a single 5-HT fiber formed varicosities over the layers. Then, do 5-HT fibers make synapses onto different interneurons in different layers? To address the question, we analyzed serial confocal images of sections immunostained for 5-HT, CB, and TH, and identified the contact sites between a 5-HT axon and CB-ir or TH-ir neurons. Serial ultra-thin sections of the contact sites were made and a series of montages were recorded. Then, we examined the contact sites through reconstruction of the 5-HT axon labeled with DAB and neurons contacting it. Direct correlative observation of CLSM (Fig. 9A) and serial EM (Fig. 9B) confirmed that the synapses were present corresponding contact sites of CLSM, and that the target

neurons of the 5-HT synapses were CB-ir and TH-ir neurons (Fig. 9E and 9F, respectively). These findings suggest that 5-HT neurons made synapses at different sites throughout a glomerulus.

Co-localization with VGLUT3

5-HT neurons express VGLUT3 (Hioki et al., 2010). The candidate of neurotransmitter released from asymmetrical synapses is glutamate. We analyzed whether 5-HT neurons co-localize with VGLUT3. The results of the CLSM study elucidated that some 5-HT-ir axons with various sizes of varicosities expressed VGLUT3 in the GL (Fig. 10A, B, C). Confirming a previous report (Hioki et al., 2010), VGLUT1 and VGLUT2 were not expressed in 5-HT-ir axons in our study (data not shown). In addition, our EM analysis revealed that 60% of 5-HT-ir axons co-localized with VGLUT3 (43 of 71 neuronal profiles, searched in 190 μm × 150 μm area, Fig. 10D) and 5-HT-ir axons co-localizing with VGLUT3 formed asymmetrical synapses (Fig. 10E).

Discussion

Using single neuron tracing, correlative CLSM, and serial EM, we revealed for the first time: (1) complete 5-HT projecting fibers from DRN to the OB through variable brain regions, (2) that a single 5-HT axon simultaneously forms synaptic contacts with different chemically defined bulbar interneurons within a glomerulus, and (3) glutamate is released from 5-HT synapse terminals. These results indicated that 5-HT neurons co-innervated heterogeneous subpopulations of chemically defined interneurons at the same time, thus further implicating 5-HT neuronal function in activating olfactory neural circuit.

Methodological consideration

A previous morphological study reported that projecting fibers of 5-HT from the DRN to the OB was three times or more greater than those in the MRN (Mclean and Shipley, 1987). 5-HT fibers in the cortex have two distinct populations; one is fine fibers with many branches from the DRN, and the other is thick varicose fibers from the MRN (Kosofsky and Molliver, 1987). Mclean et al. described thin fibers distributed in the infraglomerular layer and thick fibers with more numerous and larger varicosities distribute in the GL (Mclean and Shipley, 1987). In the present study, our initial focus is on the DRN due to increased number of DRN neurons over MRN neurons projecting to the OB. Characterizing MRN neurons and neuronal targets with a broader discussion of total 5-HT inputs and OB modulation presents an opportunity for future study. As a building block in this understanding of OB regulations, our study characterized fiber types that projected to the OB from DRN, and we thus focus on our conclusions for the DRN findings.

Sindbis viral vector is useful for single neuron traces (Kuramoto et al., 2009; Ohno et al., 2012). We showed the 5-HT projection pathway, but it was occasionally unclear for the terminals. Therefore, for more accurate visualization, we used Slc6a-cre mice and AAV vectors newly developed to express GFP in 5-HT neurons specifically. Using these methods, we reconstructed an entire image of a 5-HT fiber, consistent with

the results with sindbis viral vector. Moreover, the morphological properties of 5-HT fibers labeled with AAV vectors were similar to that shown previously with immunohistochemistry, such as the thickness of axon and distribution of varicosities. Whereas immunohistochemistry labeled numerous 5-HT fibers, viral vector-methods restrict the number of labeled fibers, enabling identification of a single fiber and resulting in whole detailed fiber morphology.

Serotonergic regulation of OB function

(1) Centrifugal regulation of interneurons

Afferent neurons from other brain regions, expressing neurotransmitters such as serotonin, noradrenalin, and acetylcholine innervate not only the OB but also other brain regions to modulate various brain functions (George et al., 2012). The primary mode of 5-HT transmission is through volume transmission (Umbriaco et al., 1995; De-Miguel and Trueta, 2005). In this mode, 5-HT nondiscriminately regulates brain function. 5-HT is released at extrasynaptic sites despite the absence of postsynaptic targets resulting in paracrine effects (De-Muguel and Trueta, 2005). However, 5-HT neurons also provide significant neuromodulation through direct synaptic transmission with target neurons (Freund et al., 1990; Dori et al., 1998; Wang et al., 2000; Muller et al., 2007; De-La-Roza and Reinoso-Suarez, 2009; Huo et al., 2009). Gracia-Llanes et al. (2010) reported that 5-HT neurons make asymmetrical synapses in the GL and targets both GABA-immunopositive and -immunonegative neurons (Gracia-Llanes et al., 2010). Type 1 periglomerular cells, containing TH and NOS, are GABA-immunopositive and innervated by olfactory receptor neurons. Conversely, type 2 periglomerular cells, containing CB and CR, are GABA-immunonegative and less innervated by olfactory receptor neurons (Kosaka and Kosaka, 2005). We showed that 5-HT neurons made asymmetrical synapses onto specific subpopulations of chemically defined interneurons of the OB. The dendrites of mitral/tufted cells are readily distinguishable from those of interneurons: large profile of regular outline with clear cytoplasm often containing small round vesicles (Pinching and Powell, 1971a, b;

Gracia-Llanes et al., 2010). A previous morphological study suggested that 5-HT neurons make synapses onto mitral/tufted cells (Gracia-Llanes et al., 2010); however, we could not distinguish mitral/tufted cells from interneurons because mitral/tufted cells do not have a specific chemical marker. Thus it is yet to be determined whether 5-HT fibers form synapses on mitral/tufted cells. Another previous report described that 8% of 5-HT synapses were made onto pyramidal cell dendrites of monkey prefrontal cortex (Smiley and Goldman-Rakic, 1996). Together, our results and previous study suggest that 5-HT neurons may rarely make synapses onto mitral/tufted cells.

The effect of 5-HT neurons on interneurons may vary considering 5-HT neurons make asymmetrical synapses onto CB-ir, CR-ir, and TH-ir neurons in the GL. From morphological findings, it could be suggested that type 2 CB-ir and CR-ir interneurons neurons might conduct recurrent modulation to projection neurons by reciprocal synapses (Toida, 2008), and TH-ir neurons, type 1 periglomerular cells, might play a role in lateral inhibition through serial synapses among projection neurons (Toida, 2008). We showed that a single 5-HT neuron made synapses onto both type 1 and type 2 periglomerular cells within a glomerulus; therefore, regulating different glomerular functions mainly associated with odor discrimination and sensation, respectively. Moreover, 5-HT neurons make synapses in the GCL, whose interneurons regulate the output from mitral/tufted cells.

As described in the results, 28% of varicosities of 5-HT neurons made synapses, consistent with previously published results (Freund et al., 1990; Smiley and Goldman-Rakic, 1996; Alvarez et al., 1998). Although there were no statistical differences in the number of varicosities of a single 5-HT fiber in each layer, there were statistical differences in the density of 5-HT fibers due to more bifurcations in the GL than the EPL and GCL. This indicates that there were more synapses in the GL compared to the other layers. Every synapse was at a varicosity, thus varicosities were considered to be the release sites of 5-HT. The fact that a single 5-HT axon made synapses within multiple glomeruli indicated that 5-HT might regulate multiple

glomerular activities simultaneously. In addition, a single 5-HT neuron ran through the GCL to the GL, suggesting OB activation along the columnar organized functional unit, which extended over a glomerular unit (Willhite et al., 2006).

5-HT activity depends on the circadian rhythm (Corthell et al., 2013) and activates most strongly in the brain during waking. The OB also has circadian rhythm (Daniel et al., 2006). It is worth examining such interesting relationships between the functions of the OB and the distribution of 5-HT fibers from other brain regions, which may be investigated in our future study.

(2) VGLUT3 in 5-HT neurons

Three vesicular transporters (VGLUT1-3) have been characterized as selective markers of glutamatergic synapses (Fremeau et al., 2002; Gras et al., 2002). VGLUT1 and 2 are expressed in glutamatergic neurons. In the OB, the dendrite and axon collaterals of projection neurons express VGLUT1 (Gabellec et al., 2007), axon terminals of olfactory receptor neurons express VGLUT2 (Gabellec et al., 2007), and VGLUT3 has a very restricted localization found in GABAergic neurons (Fremeau et al., 2002), cholinergic neurons (Gras et al., 2002), and 5-HT neurons (Hioki et al., 2004). Previous studies reported that 5-HT neurons expressed VGLUT3 in the OB (Shutoh. et al, 2008), while another study reported the absence of VGLUT3 expression by 5-HT neurons in the OB (Gabellec. et al, 2007). Existence of VGLUT3 in 5-HT neurons in the OB remains controversial; however, 5-HT neurons express VGLUT3 in the DRN as revealed by in situ hybridization (Hioki et al., 2010). We confirmed by double-immunolabeling EM that 5-HT axons co-localized with VGLUT3 in the OB. The functional relationship between 5-HT and glutamate in the same synapse remains to be clarified, but will be investigated in our future study.

Concluding remarks

Using single tracing study, correlative CLSM, and serial-EM, we revealed whole 5-HT neurons, fibers, and synapses. Our results suggest that 5-HT is the activating system of OB neural circuits. Thus, together with our previous findings, we propose a functional

scheme as summary of the present study for 5-HT neurons, originating from DRN, projecting to the OB, and activating bulbar interneurons in each layer across multiple glomeruli (Fig. 11).

Acknowledgments

We thank Prof. Takeshi Kaneko of Kyoto University for providing palGFP sindbis viral vector, Dr. Kazuto Kobayashi of Fukushima Medical University for providing TH-GFP mice, Dr. Eriko Kuramoto of Kawasaki Medical School for technical advice about viral injection, and Dr. Stephanie Parrish-Aungst of the University of Maryland School of Medicine for valuable comments and proofreading of this manuscript. Dr. Kazuyoshi Murata and Dr. Tasuo Arii of National Institute for Physiological Sciences at Okazaki, Japan for high voltage electron microscopy (H-1250M)

Conflict of interest

All authors do not have a conflict of interest.

Role of authors

All authors had full access to all the data in the study and take responsibility for the integrity of the data and the accuracy of the data analysis. Study concept and design: Kazunori Toida. Acquisition of data: Yoshinori Suzuki and Jaerin Sohn. Analysis and interpretation of data: Yoshinori Suzuki, Emi Kiyokage, and Kazunori Toida. Drafting of the manuscript: Yoshinori Suzuki. Critical revision of the manuscript for important intellectual content: Emi Kiyokage and Kazunori Toida. Statistical analysis: Yoshinori Suzuki. Obtained funding: Yoshinori Suzuki, Emi Kiyokage, Jaerin Sohn, Hiroyuki Hioki, and Kazunori Toida. Administrative, technical, and material support: Kazunori Toida and Emi Kiyokage. Study supervision: Kazunori Toida.

Literature Cited

Alvarez FJ, Pearson J'C, Harrington D, Dewey D, Torbeck L, Fyffe REW. 1998. Distribution of 5-hydroxytryptamine-immunoreactive boutons on α-motoneurons in the lumbar spinal cord of adult cats. J Comp Neurol. 393:69-83.

Bartolomé MV, Gil-Loyzaga P. 2005. Serotonergic innervation of the inner ear: is it involved in the general physiological control of the auditory receptor? Int Tinnitus J. 11:119-125.

Bregman BS. 1987. Development of serotonin immunoreactivity in the rat spinal cord and its plasticity after neonatal spinal cord lesions. Brain Res. 431:245-263.

Celada P, Puig MV, Martín-Ruiz R, Casanovas JM, Artigas F. 2002. Control of the serotonergic system by the medial prefrontal cortex: potential role in the etiology of PTSD and depressive disorders. Neurotox Res. 4:409-419.

Celio MR, Baier W, Schärer L, Gregersen HJ, de Viragh PA, Norman AW. 1990. Monoclonal antibodies directed against the calcium binding protein Calbindin D-28k. Cell Calcium. 11:599-602.

Collier, Caryl E. Sortwell, and Brian F. Daley. 1999. Diminished Viability, Growth, and Behavioral Efficacy of FetalDopamine Neuron Grafts in Aging Rats with Long-Term Dopamine Depletion: An Argument for Neurotrophic Supplementation. J Neurosci. 19:5563-5573.

Corthell JT, Stathopoulos AM, Watson CC, Bertram R, Trombley PQ. 2013. Olfactory bulb monoamine concentrations vary with time of day. Neuroscience. 247:234-41.

Daniel Granados-Fuentes, Alan Tseng, and Erik D. Herzog. 2006. A circadian clock in the olfactory bulb controls olfactory responsivity. J Neurosci. 26:12219-12225.

De la Roza C, Reinoso-Suárez F. 2009. Ultrastructural characterization of relationship between serotonergic and GABAergic structures in the ventral part of the oral pontine reticular nucleus. Neuroscience. 164:1180-1190.

De-Miguel FF, Trueta C. 2005. Synaptic and extrasynaptic secretion of serotonin. Cell Mol Neurobiol. 25:297-312.

Dori IE, Dinopoulos A, Parnavelas JG. 1998. The development of the synaptic organization of the serotonergic system differs in brain areas with different functions. Exp Neurol. 154:113-125.

Fremeau RT Jr, Burman J, Qureshi T, Tran CH, Proctor J, Johnson J, Zhang H, Sulzer D, Copenhagen DR, Storm-Mathisen J, Reimer RJ, Chaudhry FA, Edwards RH. 2002. The identification of vesicular glutamate transporter 3 suggests novel modes of signaling by glutamate. Proc Natl Acad Sci U S A. 99:14488-14493.

Freund TF, Gulyás AI, Acsády L, Görcs T, Tóth K. 1990. Serotonergic control of the hippocampus via local inhibitory interneurons. Proc Natl Acad Sci U S A. 87:8501-8505.

Fujiyama F, Furuta T, Kaneko T. 2001. Immunocytochemical localization of candidates for vesicular glutamate transporters in the rat cerebral cortex. J Comp Neurol. 435:379-387.

Furuta T, Tomioka R, Taki K, Nakamura K, Tamamaki N, Kaneko T. 2001. In vivo transduction of central neurons using recombinant sindbis virus: Golgi-like labeling of dendrites and axons with membrane-targeted fluorescent projections. J Histochem Cytochem. 49:1497-1507.

Gabellec MM, Panzanelli P, Sassoè-Pognetto M, Lledo PM. 2007. Synapse-specific localization of vesicular glutamate transporters in the rat olfactory bulb. Eur J Neurosci. 25:1373-1383.

George B. Richerson, Gary Aston-Jones, Clifford B. Saper. 2012. The modulatory functions of the brain stem. In Kandel EC (ed): Principles of neural science 5th ed. McGraw-Hill Professional. 1038-1056.

Gomez C, Briñón JG, Barbado MV, Weruaga E, Valero J, Alonso JR. 2005. Heterogeneous targeting of centrifugal inputs to the glomerular layer of the main olfactory bulb. J Chem Neuroanat 29:238–254.

Gómez C, Curto GG, Baltanás FC, Valero J, O'Shea E, Colado MI, Díaz D, Weruaga E, Alonso JR. 2012. Changes in the serotonergic system and in brain-derived neurotrophic factor distribution in the main olfactory bulb of pcd mice before and after mitral cell loss. Neuroscience 201:20-33.

Gong S, Doughty M, Harbaugh CR, Cummins A, Hatten ME, Heintz N, Gerfen CR. 2007. Targeting Cre recombinase to specific neuron populations with bacterial artificial chromosome constructs. J Neurosci. 27:9817-9823.

Gracia-Llanes FJ, Blasco-Ibáñez JM, Nácher J, Varea E, Liberia T, Martínez P, Martínez-Guijarro FJ, Crespo C. 2010. Synaptic connectivity of serotonergic axons in the olfactory glomeruli of the rat olfactory bulb. Neuroscience 169:770-780.

Gras C, Herzog E, Bellenchi GC, Bernard V, Ravassard P, Pohl M, Gasnier B, Giros B, El Mestikawy S. 2002. A third vesicular glutamate transporter expressed by cholinergic and serotoninergic neurons. J Neurosci. 22:5442-5451.

Halász N, Shepherd GM. 1983. Neurochemistry of the vertebrate olfactory bulb. Neuroscience. 10:579-619.

Hardy A, Palouzier-Pauligan B, Duchamp A, Royet JP, Duchamp-Viret P. 2005. 5-Hydroxytryptamine action in the rat olfactory bulb: in vitro electrophysiological patch-clamp recordings of juxtaglomerular and mitral cells. Neuroscience 153:717-731.

Hioki H, Fujiyama F, Taki K, Tomioka R, Furuta T, Tamamaki N, Kaneko T. 2003. Differential distribution of vesicular glutamate transporters in the rat cerebellar cortex. Neuroscience. 117:1-6.

Hioki H, Fujiyama F, Nakamura K, Wu SX, Matsuda W, Kaneko T. 2004. Chemically specific circuit composed of vesicular glutamate transporter 3- and preprotachykinin B-producing interneurons in the rat neocortex. Cereb Cortex. 14:1266-1275.

Hioki H, Nakamura H, Ma YF, Konno M, Hayakawa T, Nakamura KC, Fujiyama F, Kaneko T. 2010. Vesicular glutamate transporter 3-expressing nonserotonergic

projection neurons constitute a subregion in the rat midbrain raphe nuclei. J Comp Neurol. 518:668-686.

Huo FQ, Chen T, Lv BC, Wang J, Zhang T, Qu CL, Li YQ, Tang JS. 2009. Synaptic connections between GABAergic elements and serotonergic terminals or projecting neurons in the ventrolateral orbital cortex. Cereb Cortex. 19:1263-1272.

Hurley LM, Devilbiss DM, Waterhouse BD. 2004. A matter of focus: monoaminergic modulation of stimulus coding in mammalian sensory networks. Curr Opin Neurobiol. 14:488-495.

Jones BJ, Blackburn TP. 2002. The medical benefit of 5-HT research. Pharmacol Biochem Behav 71:555-568.

Kataoka N, Hioki H, Kaneko T, Nakamura K. 2014. Psychological stress activates a dorsomedial hypothalamus-medullary raphe circuit dividing brown adipose tissue thermogenesis and hyperthermia. Cell Metab. 20:346-358.

Kosaka K, Kosaka T. 2005. Synaptic organization of the glomerulus in the main olfactory bulb: compartments of the glomerulus and heterogeneity of the periglomerular cells. Anat Sci Int. 80:80-90.

Kosofsky BE, Molliver ME. 1987. The serotoninergic innervation of cerebral cortex: different classes of axon terminals arise from dorsal and median raphe nuclei. Synapse. 1:153-168.

Kudo T, Uchigashima M, Miyazaki T, Konno K, Yamasaki M, Yanagawa Y, Minami M, Watanabe M. 2012. Three types of neurochemical projection from the bed

nucleus of the stria terminalis to the ventral tegmental area in adult mice. J Neurosci. 32:18035-18046.

Kuramoto E, Furuta T, Nakamura KC, Unzai T, Hioki H, Kaneko T. 2009. Two Types of Thalamocortical Projections from the Motor Thalamic Nuclei of the Rat: A Single Neuron-Tracing Study Using Viral Vectors. Cereb Cortex. 19:2065-2077.

Lazarenko RM, Milner TA, Depuy SD, Stometta RL, West GH, Kievits JA, Bayliss DA, Guyenet PG. 2009. Acid sensitivity and ultrastructure of the retrotrapezoid nucleus in Phox2b-EGFP transgenic mice. J Comp Neurol. 517:69-86.

Liu S, Aungst JL, Puche AC, Shipley MT. 2012. Serotonin modulates the population activity profile of olfactory bulb external tufted cells. J Neurophysiol. 107:473-483.

Matsushita N, Okada H, Yasoshima Y, Takahashi K, Kiuchi K, Kobayashi K. 2002. Dynamics of tyrosine hydroxylase promoter activity during midbrain dopaminergic neuron development. J Neurochem. 82:295-304.

McLean JH, Shipley MT. 1987. Serotonergic afferents to the rat olfactory bulb: I. Origins and laminar specificity of serotonergic inputs in the adult rat. J Neurosci. 7:3016-3028.

McLean JH, Darby-King A, Sullivan RM, King SR. 1993. Serotonergic influence on olfactory learning in the neonate rat. Behav Neural Biol 60:152-162.

Moriizumi T, Tsukatani T, Sakashita H, Miwa T. 1994. Olfactory disturbance induced by deafferentation of serotonergic fibers in the olfactory bulb. Neuroscience.

61:733-738.

Muller JF, Mascagni F, McDonald AJ. 2007. Serotonin-immunoreactive axon terminals innervate pyramidal cells and interneurons in the rat basolateral amygdala. J Comp Neurol. 505:314-335.

Nakamura M, Sato K, Fukaya M, Araishi K, Aiba A, Kano M, Watanabe M. 2004. Signaling complex formation of phospholipase Cbeta4 with metabotropic glutamate receptor type 1 alpha and 1,4,5-trisphosphate receptor at the perisynapse and endoplasmic reticulum in the mouse brain. Eur J Neurosci. 20:2929-2944.

Ohno S, Kuramoto E, Furuta T, Hioki H, Tanaka YR, Fujiyama F, Sonomura T, Uemura M, Sugiyama K, Kaneko T. 2012. A Morphological Analysis of Thalamocortical Axon Fibers of Rat Posterior Thalamic Nuclei: A Single Neuron Tracing Study with Viral Vectors. Cereb Cortex. 22:2840-2857

Pinching AJ, Powell TP. 1971a. The neuropil of the periglomerular region of the olfactory bulb. J Cell Sci. 9:379-409.

Pinching AJ, Powell TP. 1971b. The neuropil of the glomeruli of the olfactory bulb. J Cell Sci. 9:347-377.

Petzold GC, Hagiwara A, Murthy VN. 2009. Serotonergic modulation of odor input to the mammalian olfactory bulb. Nat. Neurosci. 12:784-791.

Puthussery T, Gayet-Primo J, Taylor WR. 2010. Localization of the calcium-binding protein secretagogin in cone bipolar cells of the mammalian retina. J Comp Neurol. 518:513-525.

Ptak K, Yamanishi T, Aungst J, Milescu LS, Zhang R, Richerson GB, Smith JC. 2009. Raphé neurons stimulate respiratory circuit activity by multiple mechanisms via endogenously released serotonin and substance P. J Neurosci. 29:3720-3737.

Schnütgen F, Doerflinger N, Calléja C, Wendling O, Chambon P, Ghyselinck NB. 2003. A directional strategy for monitoring Cre-mediated recombination at the cellular level in the mouse. Nat Biotechnol. 21:562-565.

Shepherd GM, Chen WR, Greer CA. 2004. Olfactory bulb. In G.M. Shepherd (ed): The Synaptic Organization of the Brain, 5th ed. New York: Oxford University Press, pp. 165-216.

Shipley MT, Ennis M. 1996. Functional organization of olfactory system. J Neurobiol. 30:123-176.

Shipley MT, Halloran FJ, de la TJ. 1985. Surprisingly rich projection from locus coeruleus to the olfactory bulb in the rat. Brain Res. 329:294-299.

Shutoh F, Ina A, Yoshida S, Konno J, Hisano S. 2008. Two distinct subtypes of serotonergic fibers classified by co-expression with vesicular glutamate transporter 3 in rat forebrain. Neurosci Lett. 432:132-136.

Smiley JF, Goldman-Rakic S. 1996. Serotonergic axons in monkey prefrontal cerebral cortex synapse predominantly on interneurons as demonstrated by serial section electron microscopy. J Comp Neurol. 367:431-443.

Stensrud MJ, Chaudhry FA, Leergaard TB, Bjaalie JG, Gundersen V. 2013. Vesicular

glutamate transporter-3 in the rodent brain: vesicular colocalization with vesicular γ-aminobutyric acid transporter. J Comp Neurol. 521:3042-3056.

Takashima Y, Daniels RL, Knowlton W, Teng J, Liman ER, McKemy DD. 2007. Diversity in the neural circuitry of cold sensing revealed by genetic axonal labeling of transient receptor potential melastatin 8 neurons. J Neurosci. 27:14147-14157.

Takeuchi Y, Kimura H, Sano Y. 1982. Immunohistochemical demonstration of serotonin nerve fibers in the olfactory bulb of the rat, cat and monkey. Histochemistry. 75:461-471.

Toida K, Kosaka K, Heizmann CW, Kosaka T. 1994. Synaptic contacts between mitral/tufted cells and GABAergic neurons containing calcium-binding protein parvalbumin in the rat olfactory bulb, with special reference to reciprocal synapses between them. Brain Res. 650:347-352.

Toida K, Kosaka K, Heizmann CW, Kosaka T. 1996. Electron microscopic serial-sectioning/reconstruction study of parvalbumin-containing neurons in the external plexiform layer of the rat olfactory bulb. Neuroscience. 72:449-466.

Toida K, Kosaka K, Heizmann CW, Kosaka T. 1998. Chemically defined neuron groups and their subpopulations in the glomerular layer of the rat main olfactory bulb: III. Structural features of calbindin D28K-immunoreactive neurons. J Comp Neurol. 392:179-198.

Toida K, Kosaka K, Aika Y, Kosaka T. 2000. Chemically defined neuron groups and their subpopulations in the glomerular layer of the rat main olfactory bulb: Ⅳ.

Intraglomerular synapses of tyrosine hydroxylase-immunoreactive neurons. Neuroscience. 101:11-17.

Toida K. 2008. Synaptic organization of the olfactory bulb based on chemical coding of neurons. Anat Sci Int. 83:207-217.

Umbriaco D, Garcia S, Beaulieu C, Descarries L. 1995. Relational features of acetylcholine, noradrenaline, serotonin and GABA axon terminals in the stratum radiatum of adult rat hippocampus (CA1). Hippocampus. 5:605-620.

Wang QP, Guan JL, Shioda S. 2000. Synaptic contacts between serotonergic and cholinergic neurons in the rat dorsal raphe nucleus and laterodorsal tegmental nucleus. Neuroscience. 97:553-563.

Willhite DC, Nguyen KT, Masurkar AV, Greer CA, Shepherd GM, Chen WR. 2006. Viral tracing identifies distributed columnar organization in the olfactory bulb. Proc Natl Acad Sci U S A. 103:12592–12597.

Zaborszky L, Carlsen J, Brashear HR, Heimer L. 1986. Cholinergic and GABAergic afferents to the olfactory bulb in the rat with special emphasis on the projection neurons in the nucleus of the horizontal limb of the diagonal band. J Comp Neurol. 243:488-509.

Zufferey R, Donello JE, Trono D, Hope TJ. 1999. Woodchuck hepatitis virus posttranscriptional regulatory element enhances expression of transgenes delivered by retroviral vectors. J Virol. 73:2886-2892.

Figure legends

Figure 1

Immunohistochemistry of 5-hydroxytryptamine (5-HT) neurons with the anti-5-HT antibody. (**A**) 5-HT fibers were most densely distributed in the glomerular layer (GL), moderately in the granule cell layer (GCL), and sparsely in the external plexiform layer (EPL). (**B**) In the GL, fibers were distributed in the periglomerular and glomerular regions. (**C**) In the EPL, rather smaller number of fibers with few bifurcations were present. (**D**) In the GCL, fibers projected horizontally with bifurcations to the GL. (**E**) Light microscopy image for observation of high voltage electron microscopy (HVEM). (**F, F1**) A stereo pair of HVEM images (± 8°) showing 5-HT axons in the glomerular and periglomerular regions with bifurcations and varicosities, revealing accurate diameters of varicosities and non-varicosity portion (0.86 ± 0.032 μm and 0.27 ± 0.019 μm, n=10, respectively). Scale bar is 50 μm in A; 15 μm in B, C, and D; 20 μm in E; 10 μm in F1.

Figure 2

Quantification of 5-hydroxytryptamine (5-HT) fiber density measured with pixel ratio by light microscopy in five random areas of each layer. The majority of fibers were found in the glomerular layer ($p < 0.01$, student's t test).

Figure 3

Reconstruction of 5-hydroxytryptamine (5-HT) axons (blue). Both fibers traveled from the granule cell layer (GCL) to the glomerular layer (GL) passing through the external plexiform layer (EPL). (**A**): Axon #1 bifurcated two times at the superficial layer of the GCL, and each branch ran toward the EPL vertically. An axon bifurcated within a glomerulus, and one of the axonal branches entered and ramified into the other glomerulus. Traced axon length was 390 μm in the GCL, 436 μm in the EPL, and 368 μm in the GL. The number of bifurcations in each layer was 2 in the GCL, 1 in the

EPL, and 9 in the GL. The number of varicosities per 50 μm length was 2.56 in the GCL, 2.52 in the EPL, and 4.08 in the GL. (**B**): Axon #2, without bifurcations, ascended vertically into EPL. The axon arborized with 10 branching points within a glomerulus. The axon length was 362 μm in the GCL, 252 μm in the EPL, and 511 μm in the GL. The number of bifurcations in each layer was 6 in the GCL, 0 in the EPL, and 10 in the GL. The number of varicosities per 50 μm length was 2.34 in the GCL, 5.34 in the EPL, and 3.64 in the GL. (**A, A1**) and (**B, B1**): Stereo pairs of three dimensional reconstruction images (± 8°). A red circle indicates a varicosity. Scale bar: A; 50 μm (applies to B).

Figure 4

Reconstruction of 5-hydroxytryptamine (5-HT) axons (blue) and morphometry. (**A**) Axon #3 bifurcated at the superficial layer of the granule cell layer (GCL), and one of the axonal bifurcations tracked horizontally with several branches. The other axon ascended through the external plexiform layer (EPL) and ramified several times within a glomerulus. The axon length was 777 μm in the GCL, 278 μm in the EPL, and 350 μm in the glomerular layer (GL). The number of bifurcations in each layer was 5 in the GCL, 2 in the EPL, and 7 in the GL. The number of varicosities per 50 μm length was 4.31 in the GCL, 4.67 in the EPL, and 3.57 in the GL. (**B**) Axon #4 running horizontally bifurcated in the superficial GCL, and one of the bifurcated axonal branches went through the EPL without bifurcating further. Then the axon arborized several times in the GL with the axon terminals reaching a few glomeruli. The axon length was 378 μm in the GCL, 298 μm in the EPL, and 593 μm in the GL. The number of bifurcations in each layer was 2 in the GCL, 2 in the EPL, and 12 in the GL. The number of varicosities per 50 μm length was 2.64 in the GCL, 4.19 in the EPL, and 3.29 in the GL. (**A, A1**) and (**B, B1**): Stereo pairs of three dimensional reconstruction images (± 8°). A red circle indicates a varicosity. (**C**) Mean number of the varicosities per 50 μm of the axon in each layer. There were no statistical differences among the layers. (**D**) Mean number of bifurcations in each layer. The

majority of branches were in the GL. There were statistical differences between the GL and the other two layers, GCL and EPL. Scale bar is 50 μm.

Figure 5

Three dimensional reconstruction of a single 5-hydroxytryptamine (5-HT) neuron from the dorsal raphe nuclei (DRN) to the olfactory bulb (OB). (**A-E**) Reconstruction of single 5-HT neuron by combinative infection of the wild type mice and sindbis virus. (**A**) Multiple immunolabeling for characterization of 5-HT neurons in the DRN. **A1** shows infected neurons (green), **A2** shows 5-HT (blue), **A3** shows GFP (magenta), and **A4** shows the triple overlay. (**B**) DAB-visualization in the DRN. (**C, D, E**) Three dimensional visualization of a 5-HT neuron traveling from the DRN to the OB with bifurcations. (**C**) Dorsal view. (**D**) Lateral view. (**E**) Rostral view. (**F - L**) Reconstruction of a single 5-HT neuron by combinative infection of the Slc6a4-Cre mice and AAV. (**J**) Multiple immunolabeling for characterization of 5-HT neurons in the DRN. **J1** shows infected neurons (green), **J2** shows 5-HT (magenta), **J3** shows the double overlay. (**G, H**) Three dimensional visualization of a 5-HT neuron traveling from the DRN to the OB with bifurcations. (**G**) Dorsal view. (**H**) Lateral view. (**I**) Rostral view. (**F**) In the OB, an axon traverses two glomeruli. Abbreviations: DAB; 3,3'-diaminobenjidine tetrahydrochloride, GFP; green fluorescent protein. Scale bar is 200 μm in A, B, and F; 2 mm in D, and H.

Figure 6

Synaptic features of 5-hydroxytryptamine (5-HT) neurons. Electron microscopic images of synapses in the glomerular layer (GL, **A, C**) and the granule cell layer (GCL, **B**). (**A, B**) Asymmetrical 5-HT synapse with pleomorphic synaptic vesicles, active zones (white arrows), and dense cored vesicles (double arrow heads). (**C**) Synaptic terminals of olfactory receptor neurons (arrow heads) have round vesicles and thick postsynaptic densities. (**D, E**) A stereo image pair of the synapse is shown in (**A**) using electron tomography to show the three dimensional structure of the synapse and a clear

synaptic cleft. (**F**) 0.5-nm-step re-slice image (80^{th} of 140 slices) of the synapse using electron tomography showed that the postsynaptic density was differentiated and identified as an asymmetrical synapse. Scale bar is 500 nm in A, C, and D; 200 nm in B.

Figure 7

Morphometry of postsynaptic density (PSD). There is a statistical difference between the variance of the thickness of PSD of 5-hydroxytryptamine (5-HT) neurons and that of olfactory receptor neurons (F=8.4, p=0.006, Levene test). Moreover, there was a statistical difference between means of the thickness of the PSDs (p=0.04, Welch test).

Figure 8

Targets of 5-hydroxytryptamine (5-HT) neurons. (**A**-**D**) Confocal optical images of double immunostaining showing 5-HT (green) and interneurons (magenta). (**A1**-**D1**) Double labeling electron micrographs showing 5-HT (DAB) and interneurons (gold particles). **A** and **A1** show double overlay of 5-HT and calbindin (CB) in the glomerular layer (GL). **B** and **B1** show double overlay of 5-HT and tyrosine hydroxylase (TH) in the GL. **C** and **C1**, and **D** and **D1** show double overlay of 5-HT and calretinin (CR) in the GL and the granule cell layer (GCL). Abbreviation: DAB; 3,3'-diaminobenzidine tetrahydrochloride. Scale bar is 20 μm in A; 500 nm in A1 and D1; 300 nm in B1 and C1.

Figure 9

Correlative study by confocal laser microscopy (CLSM) and serial electron microscopy (EM). (**A**) Confocal projection image of multiple immunolabeling of 5-hydroxytryptamine (5-HT, magenta) and calbindin (CB, blue) in the glomerular layer of a TH-GFP mouse. (**B**) Three-dimensional reconstruction of serial EM sections: a 5-HT axon (magenta) makes asymmetrical synapses onto TH positive dendrite (green) and CB positive dendrite (blue). Yellow marks in C2 and D2 indicate synaptic sites. **C1**

shows optical image of C. **C2** shows serially EM reconstruction, and **E** shows asymmetrical synapse from 5-HT to CB at the contact site in C1. **D1** shows optical image of D. **D2** shows serially EM reconstruction, and **F** shows an asymmetrical synapse from 5-HT to TH at the contact site in D1. Abbreviations: TH; tyrosine hydroxylase, GFP; green fluorescent protein. Scale bar is 10 μm in A, 500 nm in E and F.

Figure 10

Co-localization of 5-hydroxytryptamine (5-HT) and vesicular glutamate transporter 3 (VGLUT3). (**A-C**) Multiple immunostaining of 5-HT (green) and VGLUT3 (magenta). Some 5-HT neurons expressed VGLUT3 (white arrow head), whereas some 5-HT neurons did not (white arrow). (**D**) Electron microscopic image of double labeling for 5-HT (DAB) and VGLUT3 (gold particles). Some 5-HT neurons co-localized with VGLUT3, whereas some did not. (**E**) High magnification of box in (**D**). 5-HT neuron co-localizing with VGLUT3 made asymmetrical synapses (arrow). Abbreviation: DAB; 3,3'-diaminobenzidine tetrahydrochloride. Scale bar is 10 μm in A, 500 nm in D, and 250 nm in E.

Figure 11

Concluding scheme. Together with our previous findings, 5-hydroxytryptamine (5-HT) neurons originating from dorsal raphe nuclei (DRN) project to the olfactory bulb (OB) to excite bulbar interneurons in each layer and across multiple glomeruli. 5-HT release from DRN innervations may activate multiple glomeruli and potentially the whole OB.

Supplementary data 1

A movie of axonal projection of a single serotonergic neuron from dorsal raphe nucleus to the olfactory bulb.

Supplementary data 2

A movie reconstructed from 0.5 nm step reslice stack images by electron tomography.

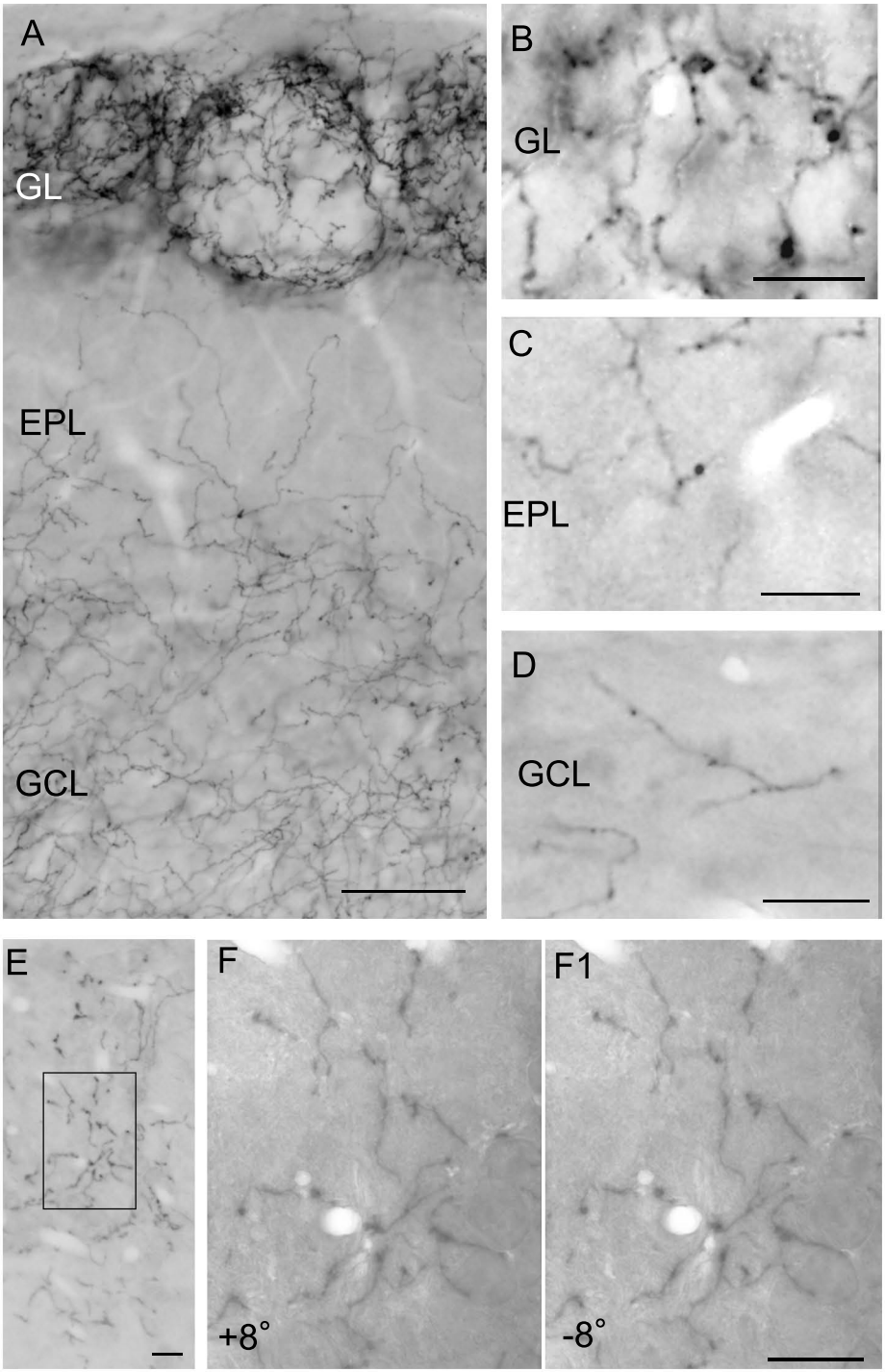
A
GL
EPL
GCL
B
GL
C
EPL
D
GCL
E
F
+8°
F1
-8°

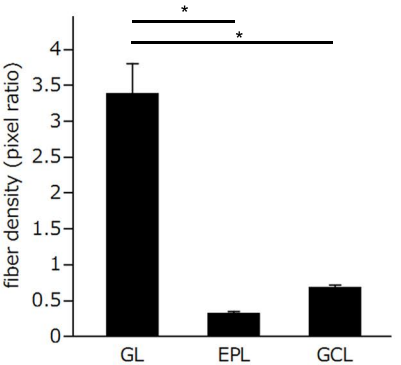
*
*
fiber density (pixel ratio)
4
3.5
3
2.5
2
1.5
1
0.5
0
GL
EPL
GCL

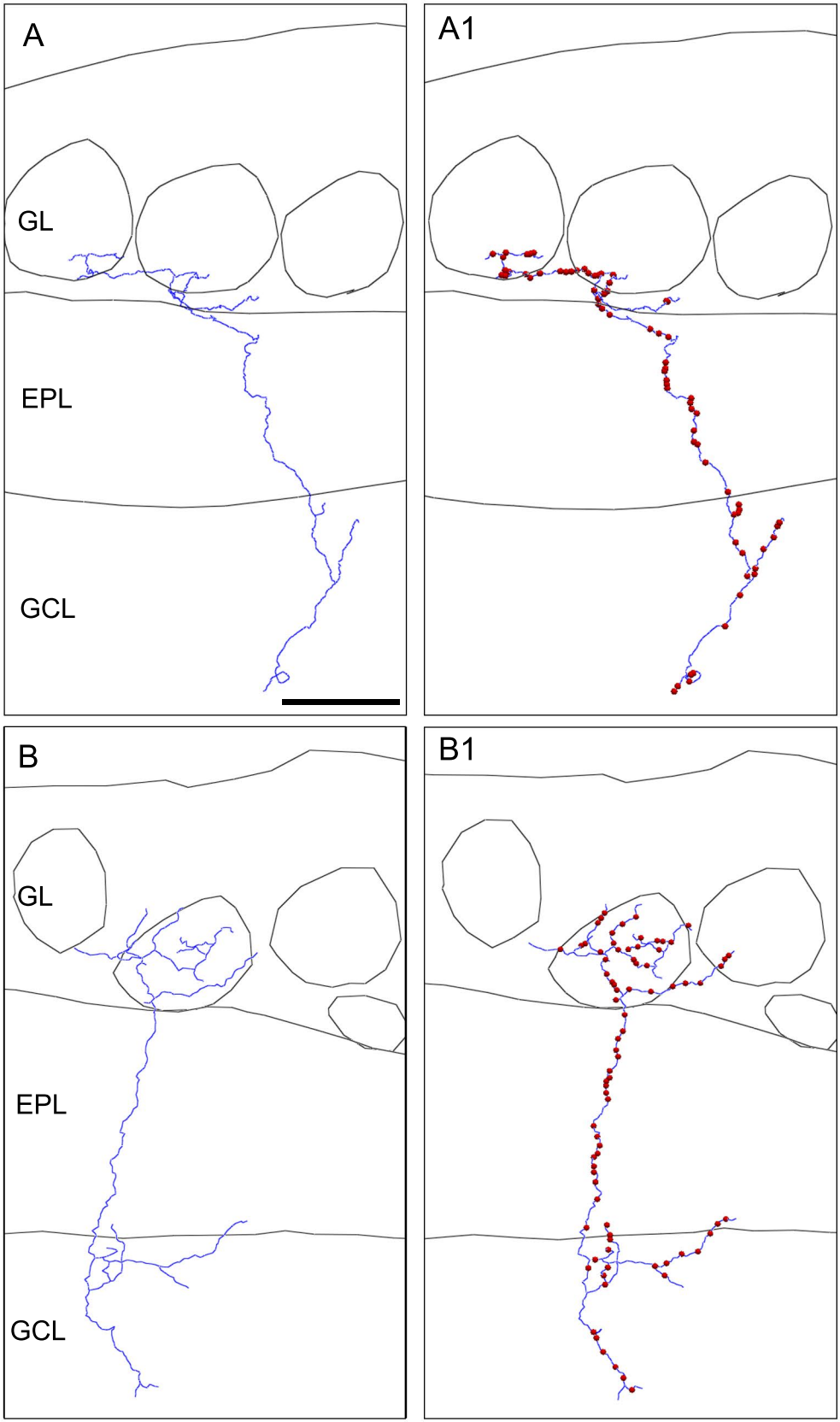
A
GL
EPL
GCL
A1
B
GL
EPL
GCL
B1

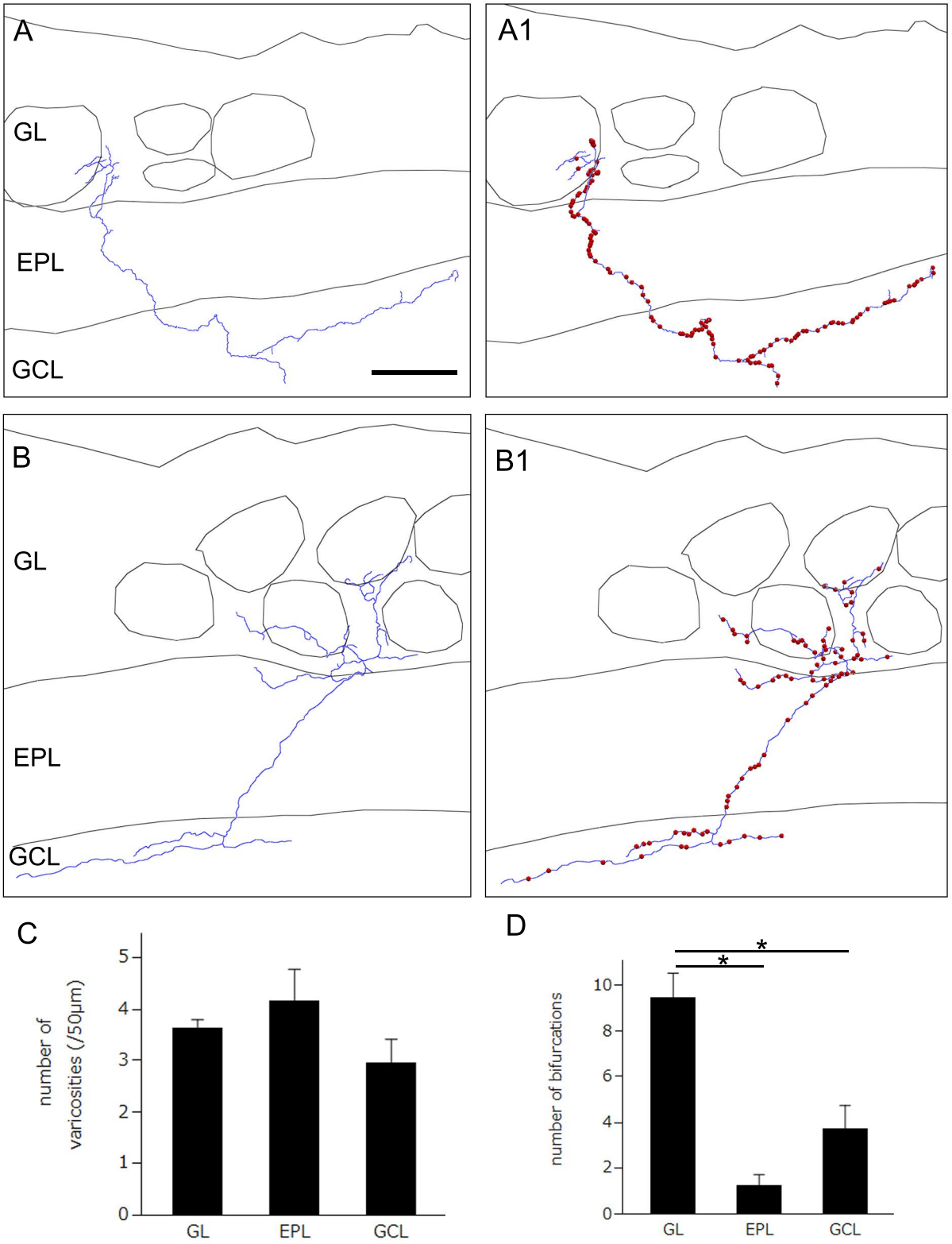
A
GL
EPL
GCL
A1
B
GL
EPL
GCL
B1
C
number of varicosities (/50µm)
0
1
2
3
4
5
GL
EPL
GCL
D
number of bifurcations
0
2
4
6
8
10
*
*
GL
EPL
GCL

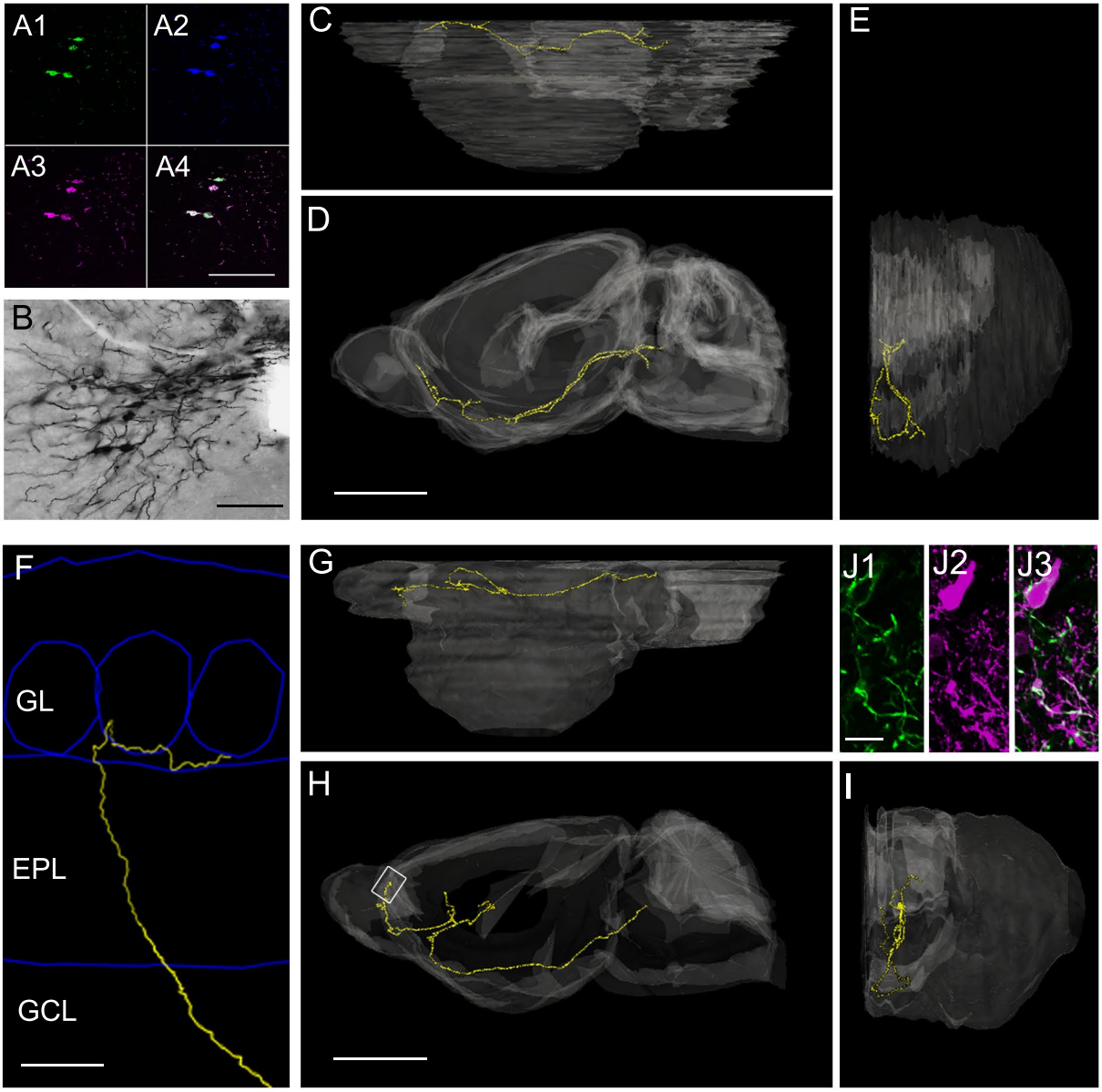
A1
A2
A3
A4
B
C
D
E
F
GL
EPL
GCL
G
J1
J2
J3
H
I

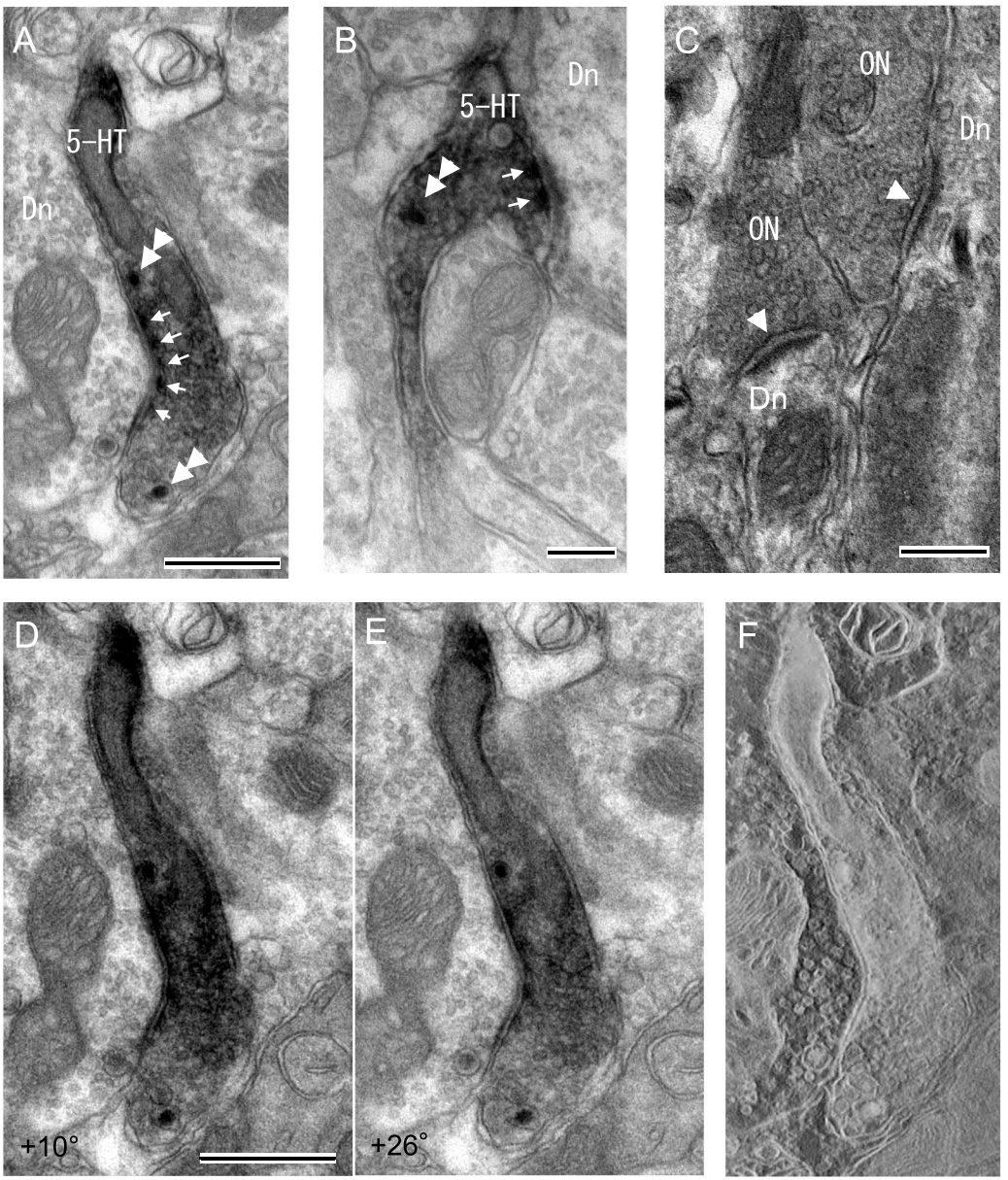
A
5-HT
Dn
B
5-HT
Dn
C
ON
Dn
ON
Dn
D
+10°
E
+26°
F

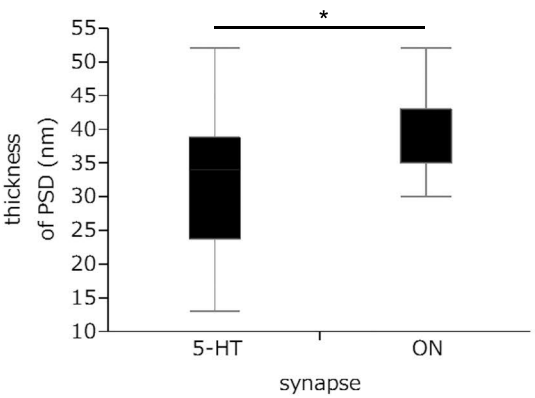
*
55
50
45
40
35
30
25
20
15
10
thickness
of PSD (nm)
5-HT
ON
synapse

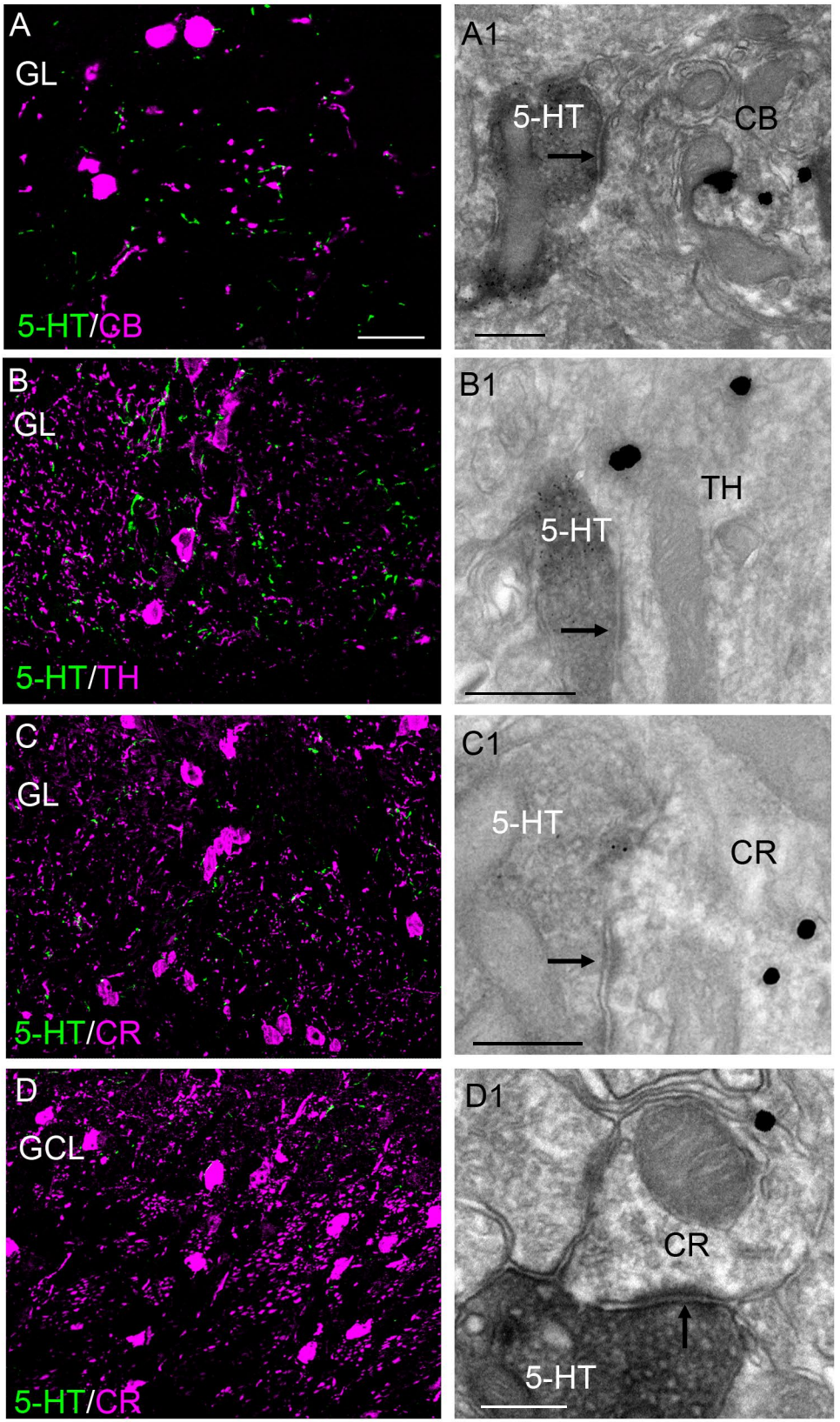
A
GL
5-HT/CB
A1
5-HT
CB
B
GL
5-HT/TH
B1
TH
5-HT
C
GL
5-HT/CR
C1
5-HT
CR
D
GCL
5-HT/CR
D1
CR
5-HT

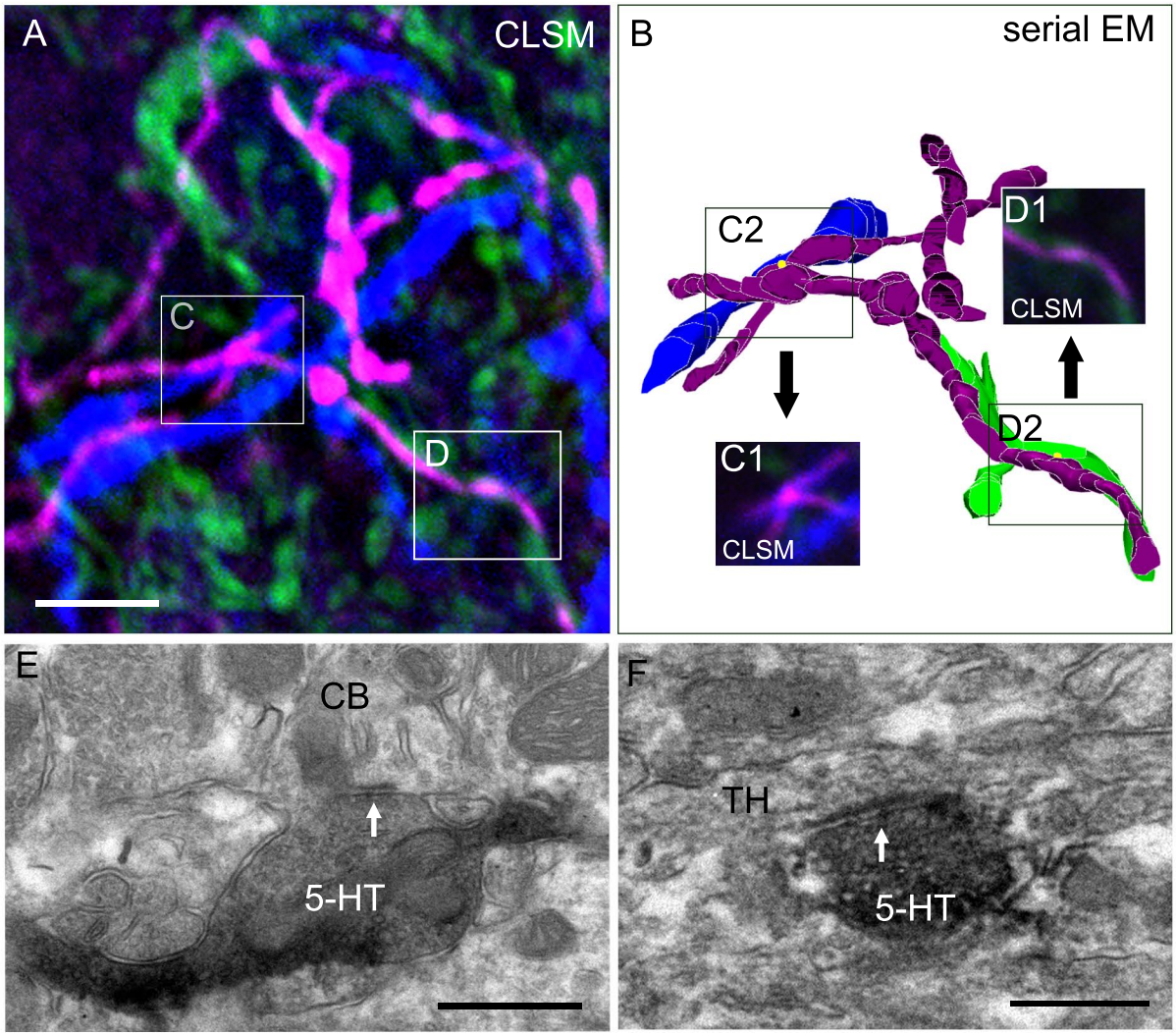
A
CLSM
C
D
B
serial EM
C2
D1
CLSM
C1
CLSM
D2
E
CB
5-HT
F
TH
5-HT

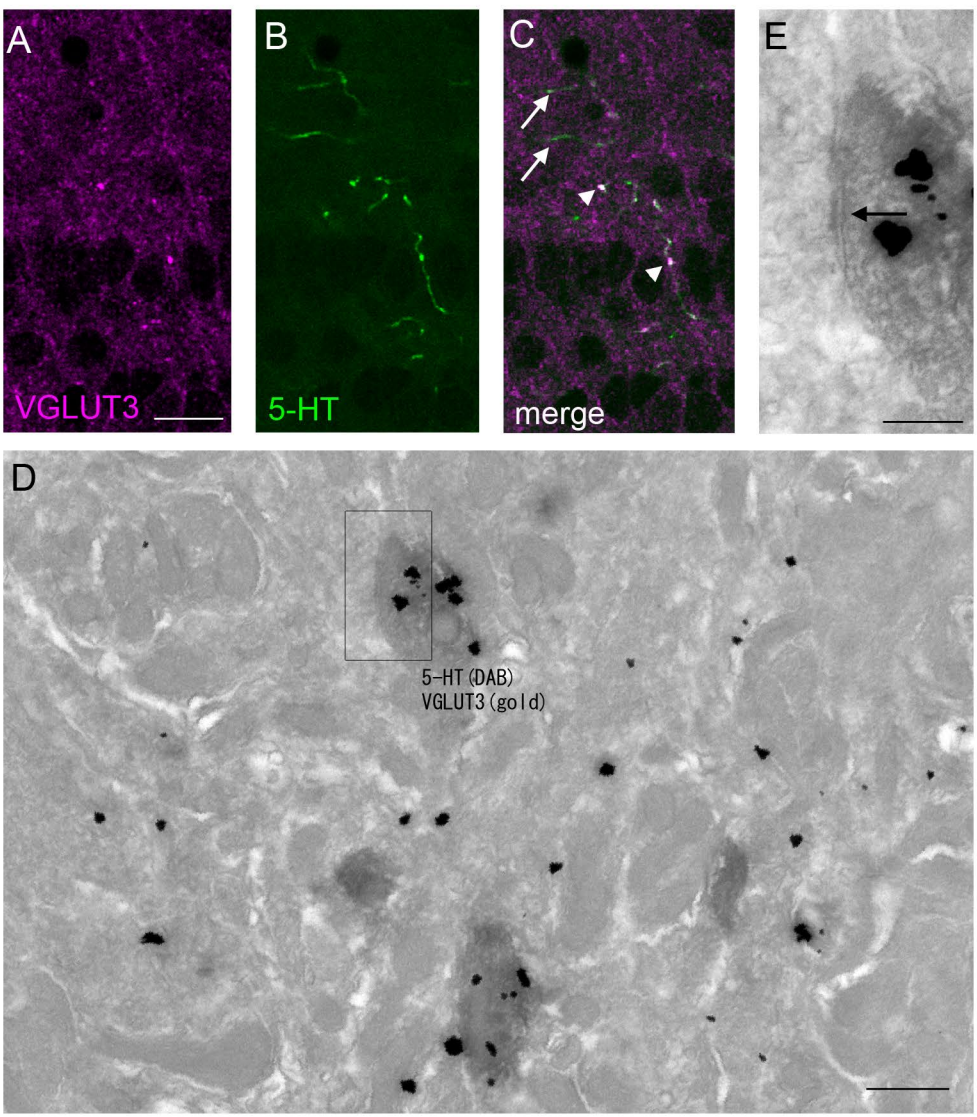
A
VGLUT3
B
5-HT
C
merge
E
D
5-HT (DAB)
VGLUT3 (gold)

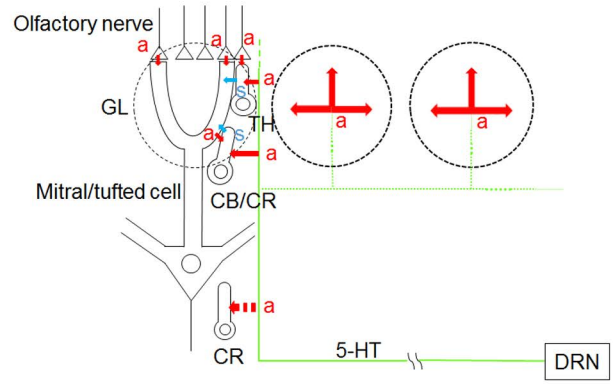
Olfactory nerve
a
a
a
GL
a
S
TH
a
S
a
Mitral/tufted cell
CB/CR
a
a
a
CR
5-HT
DRN

Table 1. Table of Primary Antibodies Used

Antigen	Description of Immunogen	Source, Host Species, Cat. #, Clone or Lot#, RRID	Concentration or dilution
5-HT	Serotonin coupled to bovine serum albumin	Immunostar, Rabbit polyclonal, Cat# 20080, Lot# 1131001, RRID:AB_572263	1:50,000
GFP	GFP isolated directly from Aequorea victoria	Life Technology, Cat# A10262, lot# 1229709, RRID:AB_11180610	0.2 μg/ml
VGLUT1	C-terminal 19 amino acids (residues 552-560) of rat VGLUT1 (CGATHSTVQPPRPPPPVRDY)	Kyoto Univ., guinea pig polyclonal, Cat# VGLUT1, RRID:AB_2315554	1 μg/ml
VGLUT2	C-terminal 29 amino acids (residues 554-582) of rat VGLUT2 (CWPNGWEKKEEFVQESAQDA YSYKDRDDYS)	Kyoto Univ., guinea pig polyclonal, Cat# VGLUT2, RRID:AB_2315571	1 μg/ml
VGLUT3	C-terminal 25 amino acids (residues 564-588) of rat VGLUT3 with N-terminal cysteine (CQQRESAFEGEEPLSYQNEEDF SETS)	Kyoto Univ., guinea pig polyclonal, Cat# VGLUT3, RRID:AB_2315581	1 μg/ml
Tyrosine Hydroxylase	An epitope on the outside of the regulatory N-terminus	Chemicon, mouse monoclonal, Cat# MAB318, lot# 25040117, RRID: AB_2315522	1:5,000
Calretinin	guinea pig calretinin	Chemicon, goat polyclonal, Cat# AB1550, lot# 0507005828, RRID:AB_90764	1:5,000
Calbindin	Whole recombinant protein of calbindin D-28K	Swant, mouse monoclonal, Cat# 300, lot# 07, RRID:AB_10000347	1:5,000
Calbindin	The last 50 amino acids of calbindin D-28K of human origin	Santa cruz, goat polyclonal, Cat# sc-7691, lot# K0311, RRID:AB_634520	0.04 μg/ml

Table 2. Summary reconstruction data of 5-HT neurons immunostained for LM.

	length (μm)			varicosities per 50 μm			number of bifurcations		
	GL	EPL	GCL	GL	EPL	GCL	GL	EPL	GCL
Axon #1	368	436	390	4.08	2.52	2.56	9	1	2
Axon #2	511	252	362	3.62	5.34	2.34	10	0	6
Axon #3	350	278	777	3.57	4.67	4.31	7	2	5
Axon #4	593	298	378	3.29	4.19	2.64	12	2	2

Abbreviations: 5-HT; 5-hydroxytryptamine, LM; light microscopy, GL; glomerular layer, EPL; external plexiform layer, GCL; granular cell layer